NASA MEMO 10-24-58L

NASA MEMO 10-24-58L

NASA MEMORANDUM

PRELIMINARY TRANSONIC PERFORMANCE RESULTS FOR SOLID AND SLOTTED TURBOJET NACELLE AFTERBODIES INCORPORATING FIXED DIVERGENT JET NOZZLES DESIGNED FOR SUPERSONIC OPERATION

By Jack F. Runckel

Langley Research Center
Langley Field, Va.

NATIONAL AERONAUTICS AND SPACE ADMINISTRATION

WASHINGTON

December 1958

NATIONAL AERONAUTICS AND SPACE ADMINISTRATION

MEMORANDUM 10-24-58L

PRELIMINARY TRANSONIC PERFORMANCE RESULTS FOR SOLID AND SLOTTED TURBOJET NACELLE AFTERBODIES INCORPORATING FIXED DIVERGENT JET NOZZLES DESIGNED FOR SUPERSONIC OPERATION*

By Jack F. Runckel

SUMMARY

An investigation of three fixed afterbody-jet exit configurations designed for supersonic speeds has been conducted in the Langley 16-foot transonic tunnel. A fixed divergent ejector, a similar ejector with longitudinal slots, and a boattail with terminal bodies extending beyond a convergent nozzle were studied. The afterbodies were installed on a pylon-supported nacelle model, and the performance of the configurations was determined at Mach numbers from 0.80 to 1.06 at an angle of attack of 0° with jet total-pressure ratios from 1 (jet off) to about 8. A hydrogen peroxide jet simulator was used to supply the hot jet exhaust. All configurations were tested without secondary air flow.

The results of the investigation indicate that the terminal-fairing configuration had the highest thrust minus drag coefficients of the three configurations at all Mach numbers and the lowest effective drag with afterburner nozzles. Flow attachment hysteresis on the divergent ejector nozzle was eliminated by the addition of longitudinal slots.

INTRODUCTION

Sufficient research has now been conducted on turbojet nozzle-afterbody combinations to define design requirements for obtaining good internal performance and low external drag for design-point operating conditions (refs. 1 and 2). In order to maintain near-optimum thrust minus drag performance as the flight and engine operating conditions are changed, however, the primary nozzle size and both the nozzle and

*Title, Unclassified.

afterbody surface shapes must be continuously variable. Such variable geometry components tend to be complex and heavy. Interest persists, therefore, in special arrangements of fixed or simply varied geometry which can be used over the desired ranges of operating conditions with acceptable performance penalties.

One type of simplified nacelle-afterbody arrangement being considered is the fixed divergent ejector in which the divergent part of the nozzle and the external nacelle lines remain fixed so that only the primary nozzle area and secondary flow rate vary. An investigation of the off-design performance of such an arrangement is reported in reference 3. The present paper reports results for a second configuration of this type. For this second configuration the divergent part of the nozzle was modified by the addition of a number of longitudinal slots ventilating it to the external flow. The purpose of these slots was to prevent nozzle flow overexpansion in off-design operation. Results also are reported for a third configuration in which still greater interaction of the internal and external flows is attained by replacing the entire nozzle and the rear boattail surfaces with six separate terminal bodies. These bodies serve the dual purpose of increasing the effective fineness ratio of the boattail and of providing rearward sloping surfaces for receiving thrust forces from the expanding jet. The rearward sloping surface of the boattail region between the terminal fairings likewise can receive thrust forces through boundary-layer—shock interaction.

The three afterbody arrangements studied were investigated on a pylon-supported nacelle model with both nonafterburner and afterburner nozzles using the hydrogen-peroxide jet simulation technique. (See ref. 4.) Tests were conducted at Mach numbers of 0.80, 0.90, 0.95, 1.00, and 1.05 with the model angle of attack of 0° and a jet pressure ratio from jet off to approximately 8. All models were investigated both with and without secondary flow. The data obtained consisted of separate thrust and drag measurements and pressure distributions in the nozzles and over the afterbodies. In order to expedite publication, only force data and selected pressure-distribution data for the zero secondary flow case are presented.

SYMBOLS

A	area, sq ft
C_D	external drag coefficient, $\frac{D}{q_\infty A_m}$
C_D'	effective drag coefficient, $C_{F,p} - (C_F - C_D)$

C_F	ejector thrust coefficient, $\frac{F}{q_\infty A_m}$
$C_{F,p}$	primary nozzle thrust coefficient, $\frac{F_p}{q_\infty A_m}$
C_p	pressure coefficient, $\frac{p - p_\infty}{q_\infty}$
D	external drag, lb
d	diameter, in.
F	ejector thrust, lb
F_p	primary nozzle thrust, lb
L	afterbody length or ejector spacing, in.
l	axial distance from exit, positive forward, in.
M	Mach number
p	static pressure, lb/sq ft
p_t	total pressure, lb/sq ft
$p_{t,j}/p_\infty$	jet pressure ratio (ratio of primary jet total pressure to free-stream static pressure)
q	dynamic pressure, lb/sq ft
r	radius, in.
x	axial distance from reference station, in.
y	afterbody radial coordinate, in.
β	boattail angle at base, deg
θ	meridian angle of afterbody, deg
ϕ	meridian angle of terminal fairing, deg

[redacted]

Subscripts:

a	original afterbody
b	base
bal	balance
e	exit of divergent nozzle, equivalent
f	primary nozzle base
m	maximum
p	primary nozzle
s	seal, slot
t	throat of divergent ejector
1	forward compartment
2	rear compartment
i	inner
o	outer
∞	free-stream conditions

Prime denotes effective value.

DESIGN CONCEPTS

Several investigations have shown that a convergent-divergent nozzle is required to obtain maximum thrust from jet engines at supersonic Mach numbers. (See refs. 1 and 2.) When the turbojet engine operates with afterburning at these speeds, secondary air is required for cooling the tailpipe, nozzle, and actuation mechanism in addition to providing efficient ejector operation. Because the boattail shape must also be continuously changed as the Mach number is varied to minimize afterbody drag, the jet-exit hardware with its overlapping plates and actuator mechanism represents a complicated apparatus having considerable weight. The following sketch indicates this type of variable nozzle-afterbody combination:

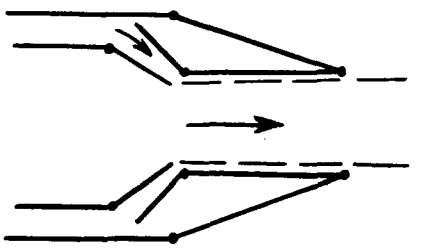

Subsonic, nonafterburning

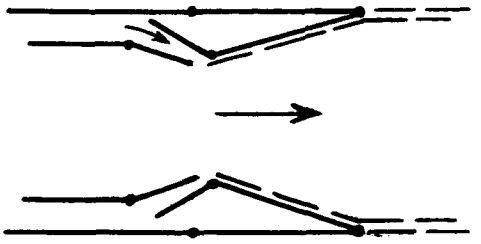

Supersonic, afterburning

Devices which simplify the exit design by eliminating the need for varying the shroud internal and external shape are, therefore, desirable providing that thrust and drag penalties are minimized.

The fixed divergent ejector is one such device that has been studied. It has been found that jet pumping and external flow effects can cause serious losses in thrust with a fixed divergent ejector when operating at off-design conditions with the jet overexpanded (ref. 3). The investigation of the present divergent ejector at transonic speeds also revealed that important internal flow hysteresis effects existed since jet detachment took place at lower pressure ratios than those for attachment. Jet pumping and attachment with a fixed divergent ejector are shown in the following sketch:

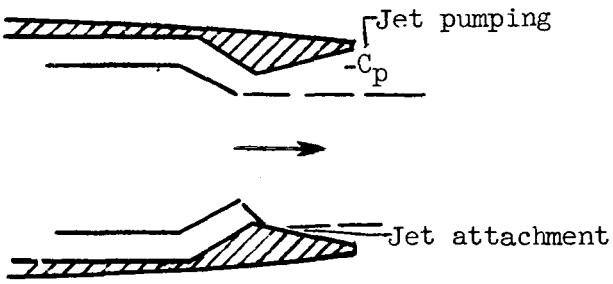

Subsonic, nonafterburning

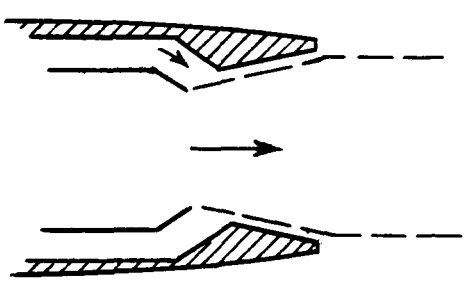

Supersonic, afterburning

[redacted]

Because of the inherent problems associated with the fixed divergent ejector in the off-design range, two fixed afterbody configurations representing attempts to overcome overexpansion and hysteresis losses were conceived. It was expected that some of the adverse effects of jet pumping on the internal surfaces could be relieved by ventilating the divergent nozzle to the external stream, since data for boattail shapes similar to the present afterbody (ref. 5) indicate that external pressures would be more positive than those on the internal surface of the present ejector. In addition, slotting could possibly eliminate local jet attachment on the divergent nozzle. A preliminary slot configuration which ventilated 20 percent of the base circumference and tapered forward to provide a thrust surface was selected. The slots extended to the throat of the divergent nozzle on the inside and to a point somewhat forward of this on the exterior surface to allow for a smooth passage for external flow into the tapered slot.

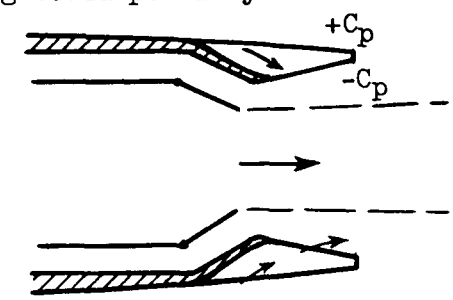

Ventilated divergent ejector
(Nonafterburning)

Another approach to the fixed jet exit configuration is the type of design that tends to integrate the external and internal stream effects to obtain acceptable performance over the speed range. Such a device is the terminal-fairing configuration which has terminal bodies extending downstream of the primary jet exit. Some preliminary work (ref. 6) with a terminal-fairing installation on a fuselage jet-exit model indicated that important decreases in afterbody drag could be achieved at supersonic and subsonic speeds. This work led to the present terminal-fairing configuration where the fixed geometry afterbody was designed for the same engine-nacelle combination as that of the fixed divergent ejector.

The use of terminal-fairing fixed geometry configurations may be beneficial in several ways. The terminal bodies increase the effective fineness ratio of the afterbody; this increase tends to reduce the pressure drag at supersonic speeds. Rearwardly decreasing cross sections of the terminal bodies provide area for the expanding jet to thrust upon at high pressure ratios. The rearward sloping boattail skirt between the terminal fairings likewise may receive thrust forces through boundary-layer—shock interaction at supersonic speeds. Where low ratios of base to maximum diameter are required, the terminal fairings can reduce the effective boattailing and base area. The secondary-air matching problem is eliminated with terminal fairings, since secondary air is only needed to cool the tailpipe, and this cooling air is vented to the base of the external boattail surface so that it does not have to flow against a

back pressure set by the primary jet. In the conventional case larger amounts of secondary air are needed for ejector action and for cooling the internal ejector surfaces. The off-design advantages of slotted afterbody-nozzle combinations, however, must be considered together with the lower on-design performance of these arrangements relative to the solid divergent ejector in order to determine the best compromise for the entire speed range.

In designing the terminal-fairing model, a reasonable compromise on the afterbody-boattail angle must be made if the drag is to be kept low at both subsonic and supersonic speeds. Transonic jet-exit investigations have indicated that the optimum boattail angle should be between 5° and 8°. (See refs. 7 and 8.) Reference 9 has shown also that the drag of such afterbodies remains reasonably low at supersonic speeds. Therefore, a body having a total area progression of boattail plus terminal fairings corresponding to a parabolic body with an equivalent boattail angle of 8° at the base was selected as a starting point. The maximum local slope of the boattail skirt between the terminal fairings was held arbitrarily to 16° and the primary nozzle was designed to change from a simple convergent shape for the nonafterburing case to a small-expansion-ratio convergent-divergent shape for the afterburning case. (This change could be accomplished practically by opening the primary nozzle lips against a short fixed skirt.)

APPARATUS AND PROCEDURE

Wind Tunnel

This investigation was conducted in the Langley 16-foot transonic tunnel, which is a single-return atmospheric wind tunnel with an octagonal slotted test section. Tunnel Mach number can be varied from low subsonic values up to about 1.08 by increasing the tunnel drive power.

Model and Support System

A sketch of the pylon nacelle jet-simulator model used in the investigation is presented in figure 1. The nacelle consisted of an ogival forebody, a cylindrical centerbody having a maximum diameter of 6.50 inches, and afterbodies which were detachable at the 47.125-inch station. The support system consisted of a conventional sting with an integral sweptforward pylon at the forward end. The nacelle was attached to the pylon through a 4-component internal strain-gage balance. A separate thrust measuring system was also mounted from the pylon support with a hydrogen peroxide jet simulator connected to the thrust balance. The jet simulator unit, which is described in reference 4, produces a

hot jet exhaust at a temperature of about 1,350° F. Jet total pressure was measured by a probe installed in the tailpipe near the primary nozzle exit. A photograph of the model installed in the Langley 16-foot transonic tunnel test section is shown in figure 2.

Afterbody Configurations

Fixed divergent ejector.- The fixed divergent ejector was designed for a stream Mach number of 2.0, a jet pressure ratio of 10.1 for an afterburner primary nozzle, and a corrected secondary weight-flow ratio of 0.042. The afterbody consisted of a curved boattail section with a small base. A sketch of this afterbody-nozzle combination is given in figure 3, and the divergent ejector parameters are presented in tables I and II.

Slotted divergent ejector.- The fixed divergent ejector was altered by cutting 8 longitudinal slots extending from the ejector throat to the exit and from the internal to external surfaces. This configuration is also illustrated in figure 3, and photographs of the slotted model are presented in figures 4 and 5. The nozzle dimensions and ejector parameters are also given in tables I and II.

Terminal fairings.- The terminal fairing model with 6 terminal bodies is shown in the photographs of figure 6, and a sketch of the configuration is presented in figure 7. The afterbody was approximately parabolic in shape with a boattail angle of 16° at the base. The effective boattail angle based on the equivalent radius of the total cross-sectional area was 8°. (See fig. 8.) The cross-sectional area of the fairings was made a maximum at the base, and the radius of each body was constant forward of the base with the radius center line becoming more submerged toward the forward end. The fairings were circular in cross section to the rear of the base with a taper based on a continuation of the fairing lines of the bodies on the boattail. A small cutoff of the design lines was necessary on the inside surface of the fairings in model construction to clear the afterburner nozzle lip. This lip had 3° of divergence beyond the throat, and the afterbody was cut back slightly to prevent impingement of the primary jet on the inside surface of the boattail.

Tests

All configurations were kept at an angle of attack of 0° throughout the Mach number range of 0.80 to 1.06. The average Reynolds number based on body length was about 20.7×10^6. The jet simulator system was operated at ratios of primary jet total pressure to free-stream static pressure from 1 (jet off) up to maximum values of about 8 for the slotted

divergent ejector and terminal fairing models and up to a maximum value of approximately 5 for the solid divergent ejector. No secondary air was supplied to the ejectors during the part of the investigation reported in this paper.

Instrumentation

Four-component force and moment measurements of the nacelle were obtained from the internal balance, but only drag measurements are reported herein. The one-component thrust balance provided a measure of the primary jet thrust. Pressures were measured on the afterbody, base, and on the divergent ejector walls and terminal bodies at the locations shown in figures 3 and 7. Total pressure and the temperature in the primary jet were also measured.

Data Reduction

Forces and pressures were converted to standard coefficients through the process described in reference 3. The drag component of the main balance measured the axial forces on the external surface of the nacelle and the force on the internal divergent ejectors plus a small internal pressure force. The thrust balance measured the primary nozzle thrust and some internal forces. The net propulsive force, or ejector thrust minus external drag, was obtained from the difference in balance readings and an internal pressure correction term:

$$F - D = F_{bal} - D_{bal} + \left(A_{s,2} - A_{s,1}\right)\left(p_1 - p_2\right)$$

The location of these balances, areas, and pressures is shown in figure 9. It should be remembered that because of the differences in physical characteristics of the primary flows (see discussion in ref. 4) the thrust minus drag coefficients determined in the tests will be somewhat different from those for a corresponding turbojet nacelle operating at the same pressure ratio. Differences in thrust minus drag coefficient, however, afford a useful comparison of the relative merit of the several configurations so long as the primary nozzle thrust areas are essentially identical. In a configuration of this type, because of the extensive aerodynamic interferences between the external and internal flow systems, it is not practical to separate the thrust and drag forces into the conventional separate quantities used in preliminary design. The total momentum of the jet flow at the sonic throat of the primary nozzle (the sonic jet thrust) is not subject to these interference effects, however, and is a basic quantity sometimes used by engine manufacturers in defining engine performance. The sonic jet thrust F_p was obtained as follows:

$$F_p = F_{bal} - (p_f - p_\infty)(A_{s,2} - A_p) + (p_1 - p_\infty)A_{s,2}$$

where the locations of the balance, areas, and pressure are shown on figure 9. With this definition of sonic jet thrust, an "effective" model drag value, useful for comparing the merits of the several configurations in familiar terms, can be obtained by subtracting the model thrust minus drag force from the sonic jet thrust:

$$D' = F_p - (F - D)$$

In the present case with zero secondary flow, the "effective" drag value is physically the conventional external drag plus the forces existing on the divergent surfaces of the exhaust nozzle. Thus, any thrust increase due to expansion of the primary jet flow appears as a reduction in effective drag; and, conversely, suction forces on the divergent part of the nozzle due to jet overexpansion or flow separation appear as increases in effective drag. With effective drag defined in this way, beneficial ejector performance appears as reduced effective drag, and ejector thrust losses appear as increased effective drag.

The effect of pylon strut support on external drag was not evaluated in this investigation, but it is believed to be small. Interference effects on all three configurations would be expected to be essentially the same, since afterbody attachment to the nacelle was identical in all cases.

Accuracy

The estimated accuracy of the data presented in this paper is as follows:

M_∞	±0.005
$p_{t,j}/p_\infty$	±0.05
C_p	±0.01
$C_F - C_D$	±0.01
$C_{D'}$	±0.01

RESULTS AND DISCUSSION

Jet Nozzle Performance

A measure of the primary jet nozzle performance is the discharge coefficient or ratio of measured weight flow to the ideal weight flow

based on the measured jet pressures and temperatures. Typical values of discharge coefficient of about 0.94 which are consistant with expected values (ref. 4) were obtained for the primary nozzle of this investigation. The ejector thrust ratio, or ratio of measured primary convergent-nozzle thrust plus divergent ejector-nozzle thrust to ideal convergent-nozzle thrust, was 0.88 for the divergent ejector model at a Mach number of 0.95 and a jet pressure ratio of 4.45 with nonafterburner nozzle. It is evident that the forces on the divergent nozzle for this typical off-design case represent a loss in ejector thrust.

Thrust Minus Drag Measurements

The thrust minus drag performance of the three fixed nozzle afterbody configurations is presented in figures 10 and 11 for the nonafterburner and afterburner nozzles, respectively. As noted in the section entitled "Data Reduction," it should be remembered that the coefficients shown are not directly applicable to the performance of airplane installations. Also, in the nonafterburner case, the thrust minus drag coefficients shown for the divergent ejector are not directly comparable to those for the other two configurations because of a small difference in primary nozzle-throat diameter. (See table II.) As shown in the next section of the paper, "Effective Drag Comparisons," the differences in thrust due to the differences in nozzle-throat area are enough to reverse the order of merit of the divergent ejector and slotted ejector configurations.

The flagged symbols in figure 10 indicate data obtained when the pressure ratio was decreased from that required to attach the jet to the divergent ejector wall. The jet remains attached to a pressure ratio lower than that required for jet attachment; therefore, overexpansion of the jet and a consequent loss in ejector thrust results. This loss is apparent at all Mach numbers. Results not presented show that this hysteresis persists with small quantities of secondary flow up to 3 percent of the primary air flow and that it can be eliminated with larger quantities of secondary air flow. No hysteresis effects were noted for the two ventilated configurations, and important flow hysteresis effects apparently did not occur in any of the afterburning configurations. (See fig. 11.)

The thrust minus drag data for the three configurations are directly comparable in the afterburning case because the primary nozzle throat areas were identical. (See table II.) In general, these data (fig. 11) show significant performance gains for the slotted-afterbody and terminal-fairing configurations over those for the solid divergent ejector. One exception is that the advantage of the ventilated ejector over the solid ejector essentially vanishes at the maximum test Mach number. (See fig. 11(d).) This change is caused presumably by the internal pressure

[redacted]

not being sufficient in the case of the slotted nozzle to prevent some inflow into the slots and thereby to increase the effective external boattail angle. (A sample pressure distribution is shown later.)

Thrust minus drag coefficients for the three nozzle-afterbody combinations are plotted against Mach number in figures 12 and 13 for a schedule of jet pressure ratios typical for an advanced turbojet engine. Within the Mach number range of the tests, the terminal-fairing configuration is shown to have provided significant gains in thrust minus drag coefficient over that for the $M_\infty = 2$ design solid divergent ejector with both nonafterburner and afterburner nozzle operation. Unpublished results indicate that the performance of the divergent ejector may be expected to improve with the use of secondary flow. Further research is required, therefore, to optimumize and evaluate the relative merit of configurations of these two types. Because of the comparison difficulties encountered for the nonafterburner case, the data of figures 12 and 13 are replotted in figures 14 and 15 in terms of the effective drag coefficient which provides a more valid comparison and relates the increments shown to a familiar reference, the nacelle drag. The effective drag coefficient was obtained by removing values of the primary nozzle sonic-thrust coefficient from the experimentally determined values of thrust minus drag coefficient.

Effective Drag Comparisons

For the nonafterburning case, it is shown in figure 14 that the effective drag coefficients for the slotted ejector are higher than those for the solid ejector, despite the reverse order of merit shown for the thrust minus drag coefficients in figure 12. As stated previously, the difference is caused by the slightly oversize primary nozzle used in the slotted configuration (table II) which provided more thrust than the smaller nozzles at any given jet pressure ratio and thus invalidated the uncorrected thrust minus drag comparisons. It should be pointed out that the divergent ejector data shown by the solid line of figure 14 represents a slight extrapolation of test results to obtain the effective drag coefficients at scheduled jet pressure ratios. These pressure ratios, however, are in the region where flow-attachment hysteresis takes place (see fig. 10(b), for example), and large increases in ejector drag can occur if the jet attaches to the walls of the divergent ejector. Values of effective drag coefficient for jet attachment are also shown in figure 14 to indicate the severe increases in drag for this condition.

Operation with afterburner nozzles (fig. 15) resulted in the terminal-fairing configuration providing effective drag coefficients lower than those of the $M_\infty = 2$ design solid divergent ejector by 19 to

33 percent. The effective drag coefficients for the divergent ejector, however, increased at subsonic speeds in going from the nonafterburner to the afterburner nozzle coefficient while the drag of the terminal-fairing model remained essentially constant. Changing to the afterburner nozzle in the slotted divergent ejector configuration resulted in a reduction in effective drag coefficient at the highest test speed. The relative performance of the solid and slotted configurations at the design point ($M_\infty = 2$) is presently unknown.

Pressure Measurements

Sample surface-pressure-distribution measurements offer a partial explanation as to the reason that slotting the divergent ejector produced detrimental effects for nonafterburner nozzle operation and favorable effects for afterburner nozzle operation. In the former case (fig. 16(a)) the effect of slotting was to increase the external pressures in the region of the base and to decrease pressures ahead of this region. This effect would be expected if external flow was entering the forward portions of the slots. At the subsonic Mach number, internal pressures, except near the exit, were lower for the slotted configuration because the slots vented the interior space to a boattail pressure lower than the base pressure of the solid ejector configuration. At the supersonic speeds the pressures on the divergent nozzle increased with slotting, but the increase apparently was not enough to overcome the reduction in external boattail pressure.

For the afterburner nozzles (fig. 16(b)), the pressure distributions on the external surface solid and slotted ejector configuration are similar to those for the nonafterburner nozzle. However, large increases in internal pressure occur for the slotted configuration because of a reduction in overexpansion of the internal flow which is directly chargeable to ventilation of the internal surfaces by the slots. The results of figure 16 indicate that shorter slots extending from the exit forward about halfway to the throat may provide increases in performance with both sizes of primary nozzles by reducing both the external and internal drag from the value of the fixed divergent ejector.

The improved performance of the terminal-fairing configuration relative to the performance of the solid and slotted ejector configurations is attributed to the change in effective boattail shape. This change both reduced the boattail pressure drag and increased the pressure acting on the engine base (the annular area between the nozzle and shroud diameter, fig. 7) by increasing the average level of pressure of the flow to which this base was effectively vented. For the range of conditions shown in figures 14 and 15, the primary nozzle base pressure coefficients are presented in figure 17. The values for both the nonafterburner and

afterburner nozzles are generally considerably higher for the terminal-fairing configuration than for the other two configurations.

The superiority of the terminal-fairing configuration to the others in the afterburner nozzle case undoubtedly arises from the same sources as in the nonafterburner case. The complexity of the shape of the terminal-fairing configuration together with the fact that the engine bases (which were useful as a region of comparison in the nonafterburning case) are essentially eliminated in the afterburning case effectively prevents satisfactory explanation of this superiority by comparison of pressures in a few local regions.

Obviously, much more work is required in order to optimumize the terminal-fairing type of design and to develop specific design rules. It is noted that the sensitivity of the ventilated-type nozzle to the boattail-flow pressure level indicates that external flow interferences between the nacelle and other parts of the airplane must be taken into account in afterbody design to a much greater extent than is customary for most solid-nozzle installations.

CONCLUDING REMARKS

The results of the present preliminary investigation of the transonic performance of turbojet nacelle afterbodies, incorporating fixed divergence geometry jet nozzles designed for supersonic operation, indicate that substantial performance gains can be obtained in off-design operation by properly designed afterbody slots. The "terminal fairing" configuration studied provided effective drag coefficients lower than those for a Mach number 2 design solid walled divergent-ejector afterbody by 19 to 33 percent in the afterburner nozzle case. Flow hysteresis and secondary-flow matching problems also are eliminated with this type of design.

The performance of a slotted afterbody in design point operation is presently unknown. The design requirements for slotted afterbodies also are not well understood beyond the basic requirement that the external part of the slotted surface must both increase the effective fineness ratio of the afterbody and provide as high as possible static pressures at the outside entrances to the slots. Obviously much further research must be undertaken before the merit of the slotted afterbody can be established relative to other fixed-geometry arrangements of interest such as the fixed divergent ejector with a large amount of secondary flow.

Langley Research Center,
National Aeronautics and Space Administration,
Langley Field, Va., August 21, 1958.

REFERENCES

1. Cortright, Edgar M., Jr.: Some Aerodynamic Considerations of Nozzle-Afterbody Combinations. Aero. Eng. Rev., vol. 15, no. 9, Sept. 1956, pp. 59-65.

2. Greathouse, William K., and Beale, William T.: Performance Characteristics of Several Divergent-Shroud Aircraft Ejectors. NACA RM E55G21a, 1955.

3. Swihart, John M., and Mercer, Charles E.: Investigation at Transonic Speeds of a Fixed Divergent Ejector Installed in a Single-Engine Fighter Model. NACA RM L57L10a, 1958.

4. Runckel, Jack F., and Swihart, John M.: A Hydrogen Peroxide Turbojet-Engine Simulator for Wind-Tunnel Powered-Model Investigations. NACA RM L57H15, 1957.

5. Henry, Beverly Z., Jr., and Cahn, Maurice S.: Pressure Distributions Over a Series of Related Afterbody Shapes As Affected by a Propulsive Jet at Transonic Speeds. NACA RM L56K05, 1957.

6. Swihart, John M., Norton, Harry T., Jr., and Schmeer, James W.: Effect of Several Afterbody Modifications Including Terminal Fairings on the Drag of a Single-Engine Fighter Model With Hot-Jet Exhaust. NASA MEMO 10-29-58L, 1958.

7. Cubbage, James M., Jr.: Jet Effects on the Drag of Conical Afterbodies for Mach Numbers of 0.6 to 1.28. NACA RM L57B21, 1957.

8. Henry, Beverly Z., Jr., and Cahn, Maurice S.: Preliminary Results of an Investigation at Transonic Speeds To Determine the Effects of a Heated Propulsive Jet on the Drag Characteristics of a Related Series of Afterbodies. NACA RM L55A24a, 1955.

9. Rustemeyer, A. H., and Twomey, E. J.: Thrust and Drag Characteristics of Several Turbojet Exhaust Models at Supersonic and High Subsonic Mach Numbers. Rep. R-0922-16 (Contract NOa(s) 55-134-c), Res. Dept., United Aircraft Corp., June 1957.

TABLE I.- EJECTOR DIMENSIONS MEASURED AT AMBIENT TEMPERATURE

(a) Nonafterburner primary nozzle

Dimension	Dimensions for -		
	Divergent ejector configuration	Slotted configuration	Terminal-fairing configuration
d_p	2.12	2.19	2.19
d_e	3.92	3.92	----
d_t	3.25	3.25	----
d_b	4.23	4.23	----
L	2.40	2.46	3.35
L_t	.43	.49	----
$L_{s,i}$	----	1.98	----
$L_{s,o}$	----	3.16	----

(b) Afterburner primary nozzle

Dimension	Dimensions for -		
	Divergent ejector configuration	Slotted configuration	Terminal-fairing configuration
d_p	2.77	2.77	2.77
d_e	3.92	3.92	----
d_t	3.25	3.25	----
d_b	4.23	4.23	----
L	2.97	2.97	3.19
L_t	1.01	1.01	----

TABLE II.- EJECTOR DIMENSIONS CALCULATED FOR HOT TEMPERATURES

(a) Nonafterburning primary nozzle

Dimension	Dimensions for -		
	Divergent ejector configuration	Slotted configuration	Terminal-fairing configuration
d_p	2.15	2.22	2.22
d_e	3.96	3.96	----
d_t	3.26	3.26	----
d_b	4.25	4.25	----
L	2.22	2.28	3.15
L_t	.26	.32	----
d_e/d_p	1.85	1.78	----
d_t/d_p	1.52	1.47	----
d_b/d_p	1.98	1.91	----
L/d_p	1.04	1.03	1.42
L_t/d_p	.12	.14	----

(b) Afterburner primary nozzle

Dimension	Dimensions for -		
	Divergent ejector configuration	Slotted configuration	Terminal-fairing configuration
d_p	2.81	2.81	2.81
d_e	3.96	3.96	----
d_t	3.26	3.26	----
d_b	4.25	4.25	----
L	2.80	2.80	3.00
L_t	.84	.84	----
d_e/d_p	1.41	1.41	----
d_t/d_p	1.16	1.16	----
d_b/d_p	1.52	1.52	----
L/d_p	1.00	1.00	1.38
L_t/d_p	.30	.30	----

[redacted]

FOREBODY ORDINATES			
Station, x, in.	Radius, r, in.	Station, x, in.	Radius, r, in.
2.000	0.490	20.000	3.080
5.000	1.140	20.900	3.127
8.000	1.700	23.500	3.220
11.000	2.175	26.000	3.250
14.000	2.565	47.125	3.250
17.000	2.865		

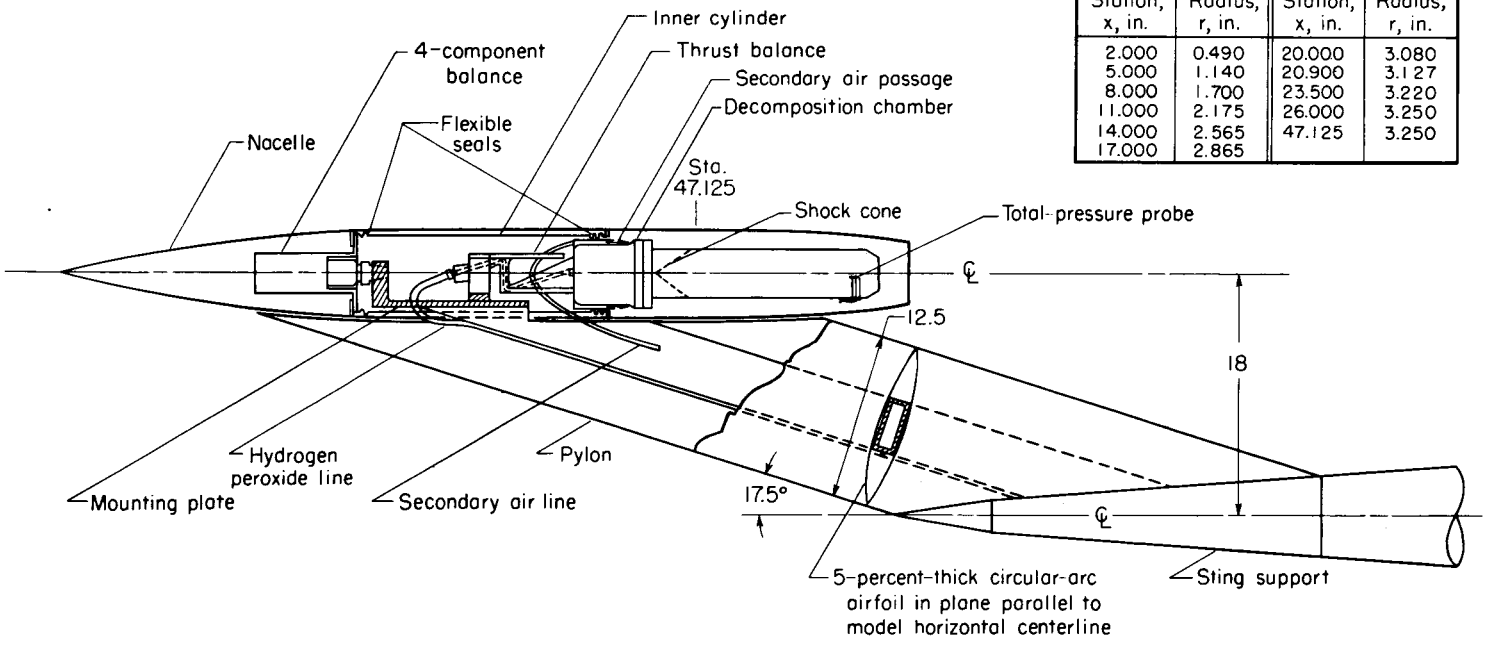

Figure 1.- Sketch of pylon-supported nacelle model. All dimensions are in inches.

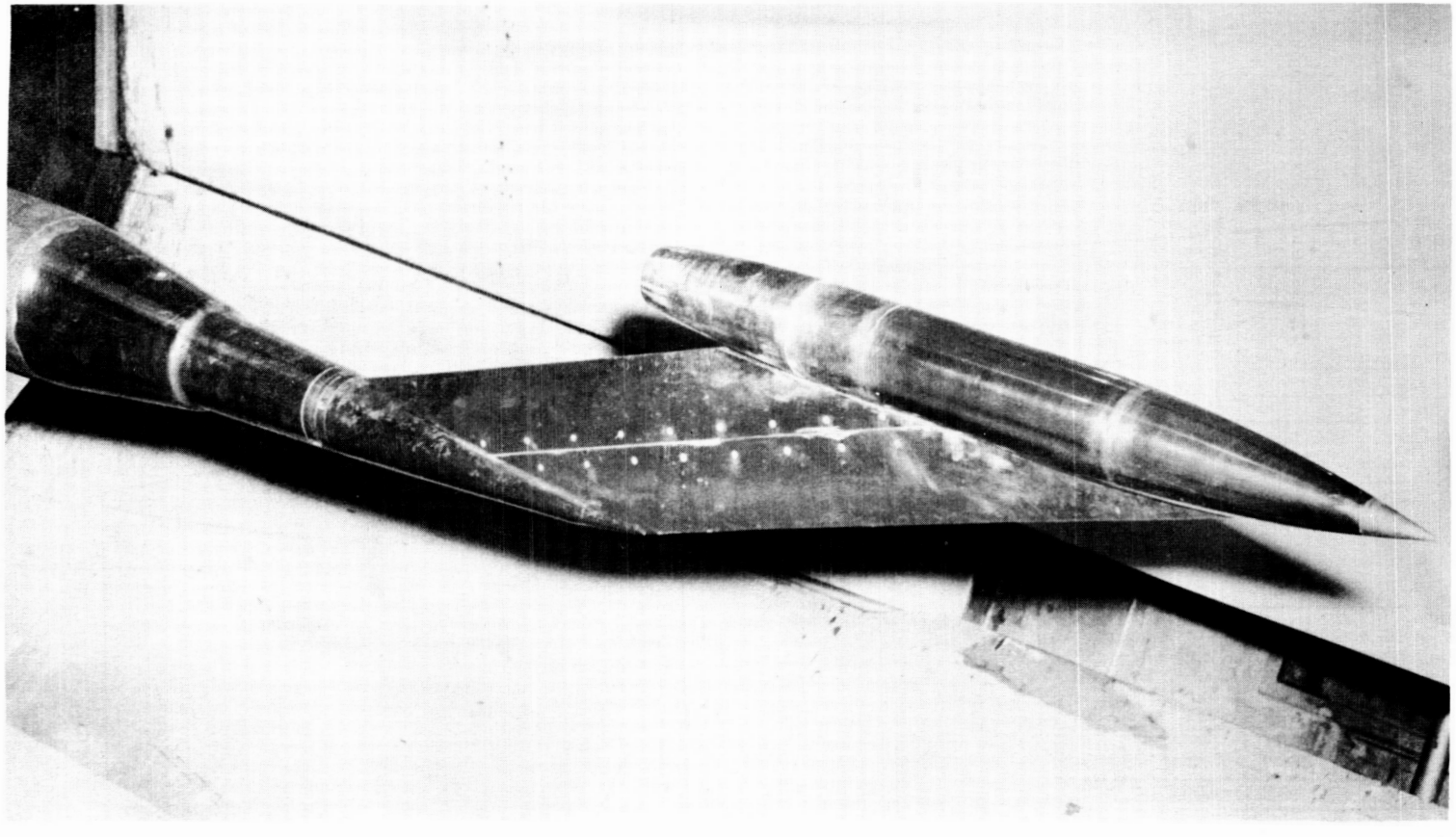

L-57-2316

Figure 2.- Photograph of pylon supported nacelle model with fixed divergent-ejector afterbody installed in the 16-foot transonic tunnel.

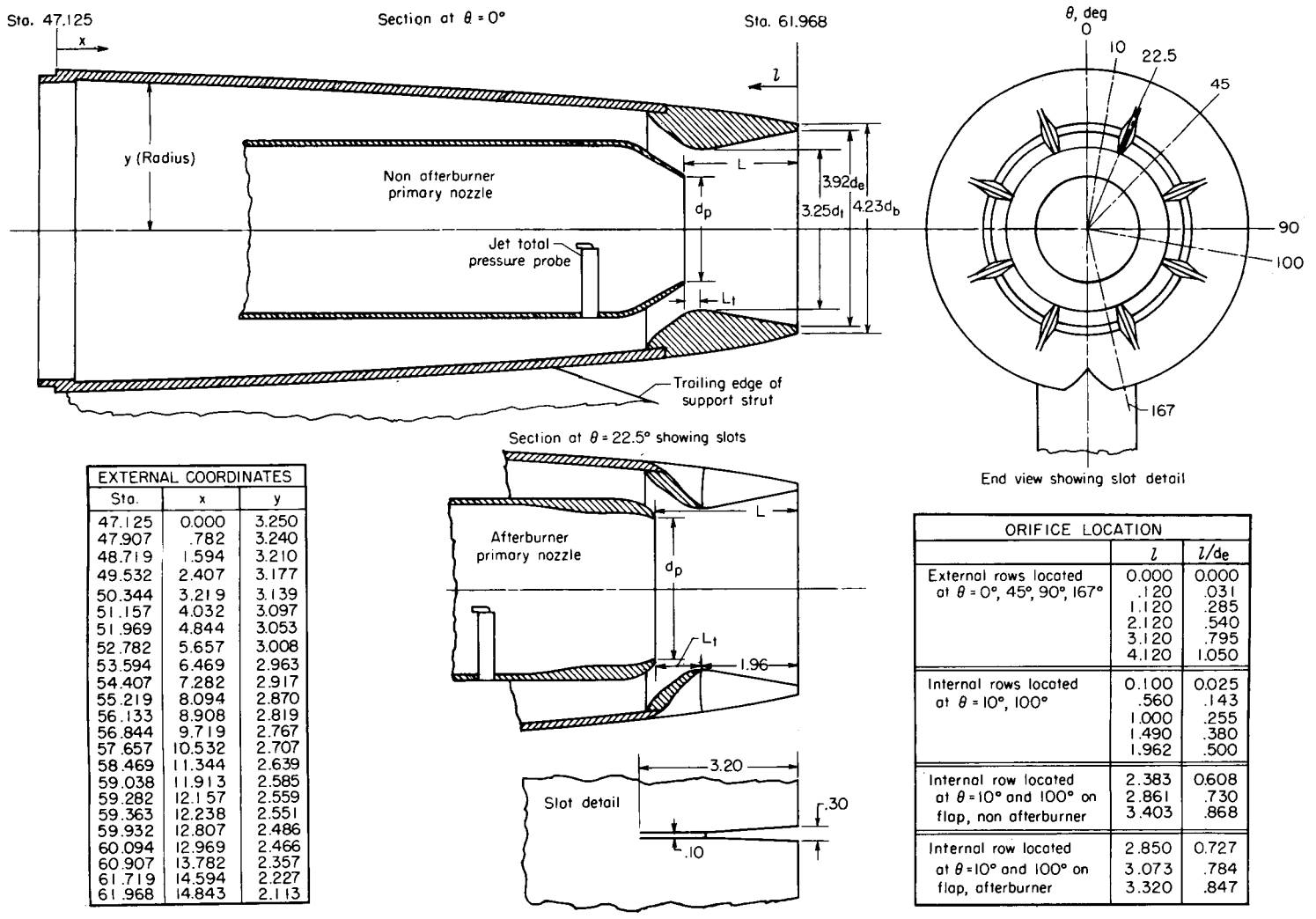

EXTERNAL COORDINATES		
Sta.	x	y
47.125	0.000	3.250
47.907	.782	3.240
48.719	1.594	3.210
49.532	2.407	3.177
50.344	3.219	3.139
51.157	4.032	3.097
51.969	4.844	3.053
52.782	5.657	3.008
53.594	6.469	2.963
54.407	7.282	2.917
55.219	8.094	2.870
56.133	8.908	2.819
56.844	9.719	2.767
57.657	10.532	2.707
58.469	11.344	2.639
59.038	11.913	2.585
59.282	12.157	2.559
59.363	12.238	2.551
59.932	12.807	2.486
60.094	12.969	2.466
60.907	13.782	2.357
61.719	14.594	2.227
61.968	14.843	2.113

ORIFICE LOCATION		
	l	l/de
External rows located at θ = 0°, 45°, 90°, 167°	0.000 .120 1.120 2.120 3.120 4.120	0.000 .031 .285 .540 .795 1.050
Internal rows located at θ = 10°, 100°	0.100 .560 1.000 1.490 1.962	0.025 .143 .255 .380 .500
Internal row located at θ = 10° and 100° on flap, non afterburner	2.383 2.861 3.403	0.608 .730 .868
Internal row located at θ = 10° and 100° on flap, afterburner	2.850 3.073 3.320	0.727 .784 .847

Figure 3.- Sketch of divergent-ejector afterbody and details of slotted configuration. See table I for ejector dimensions. All dimensions are in inches.

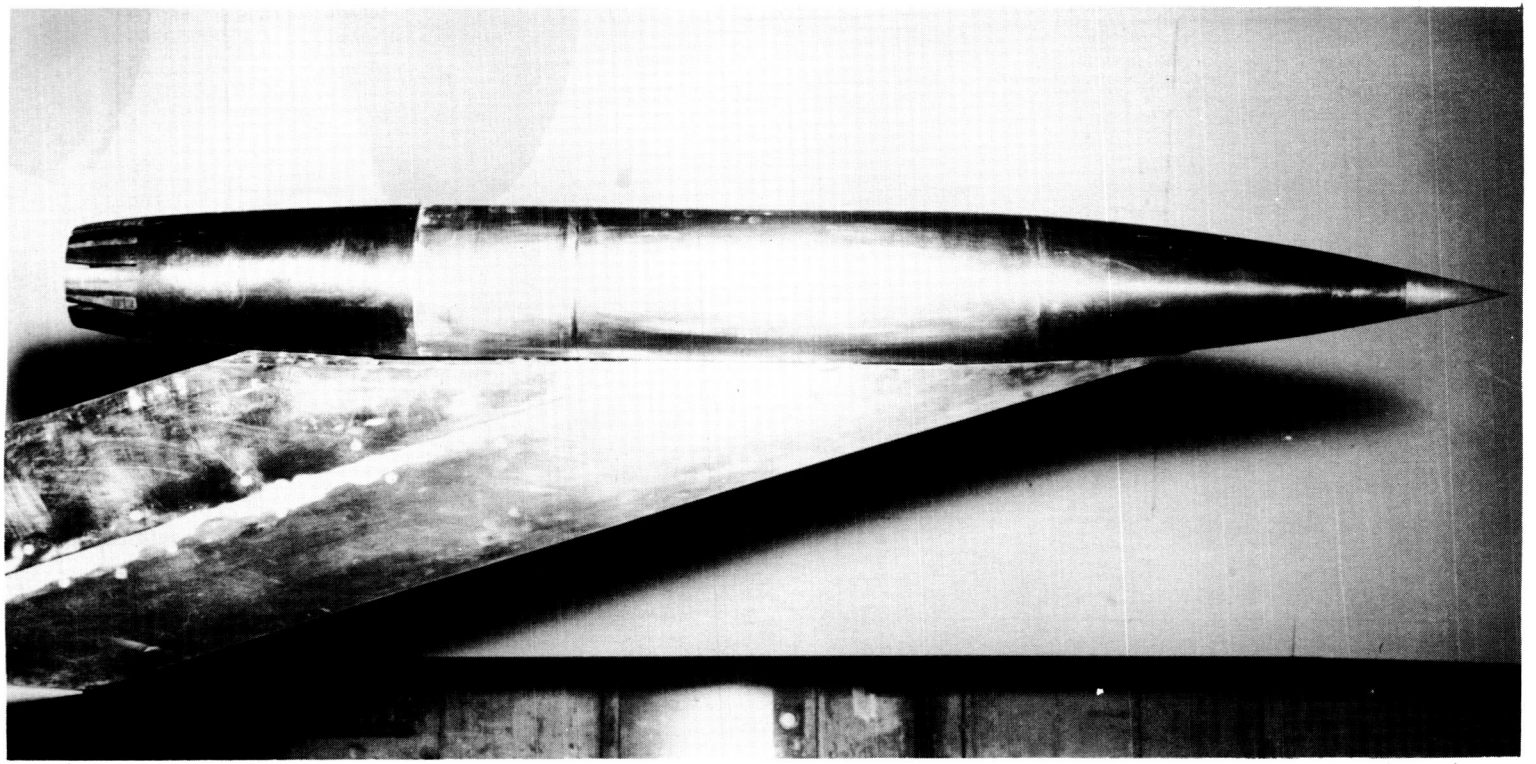

L-58-423

Figure 4.- Photograph of slotted afterbody on pylon-supported nacelle model.

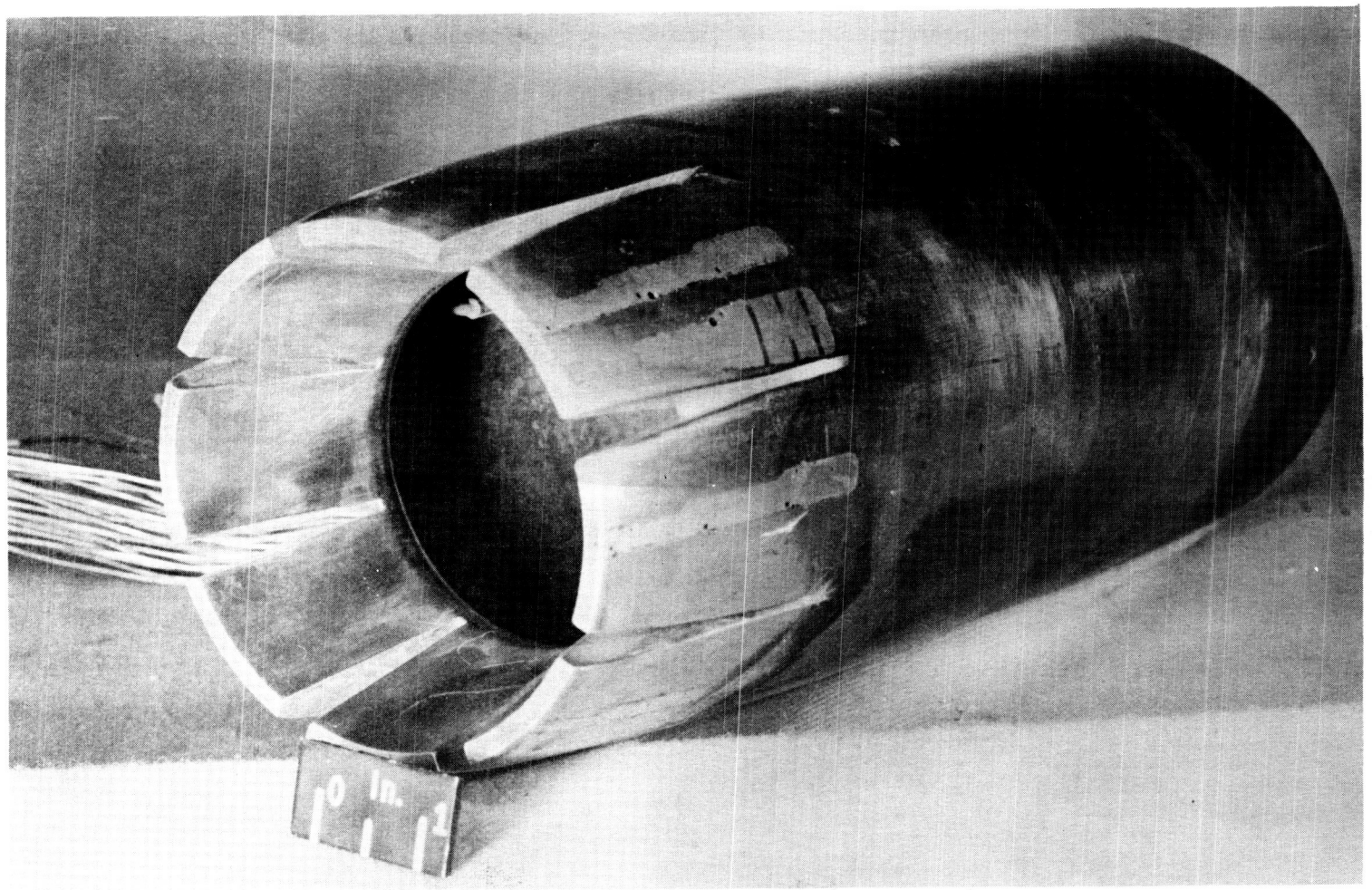

Figure 5.- Closeup view of slotted afterbody. L-58-623

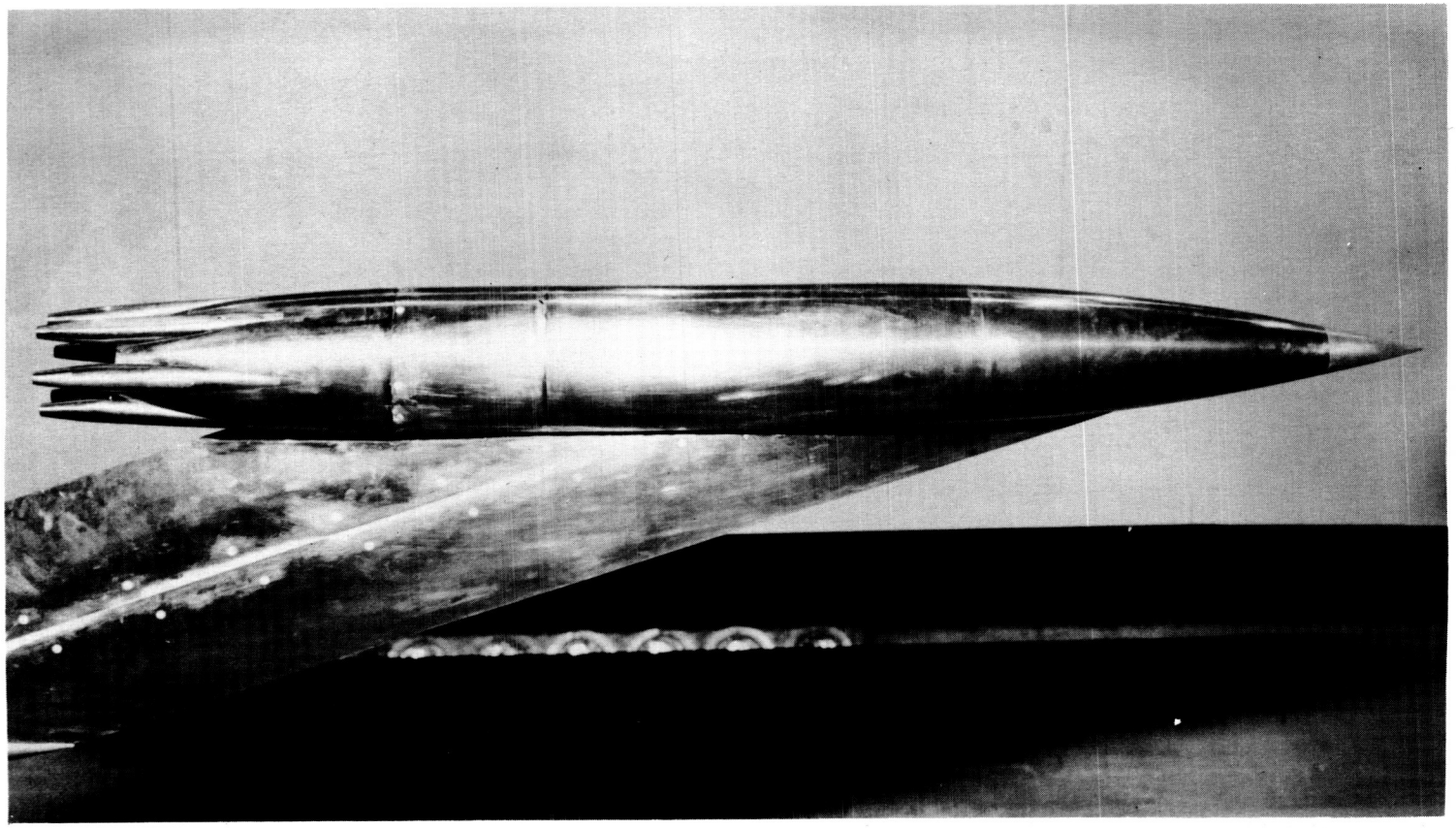

(a) Side view.

L-58-217

Figure 6.- Photograph of afterbody with terminal fairings on pylon-supported nacelle model.

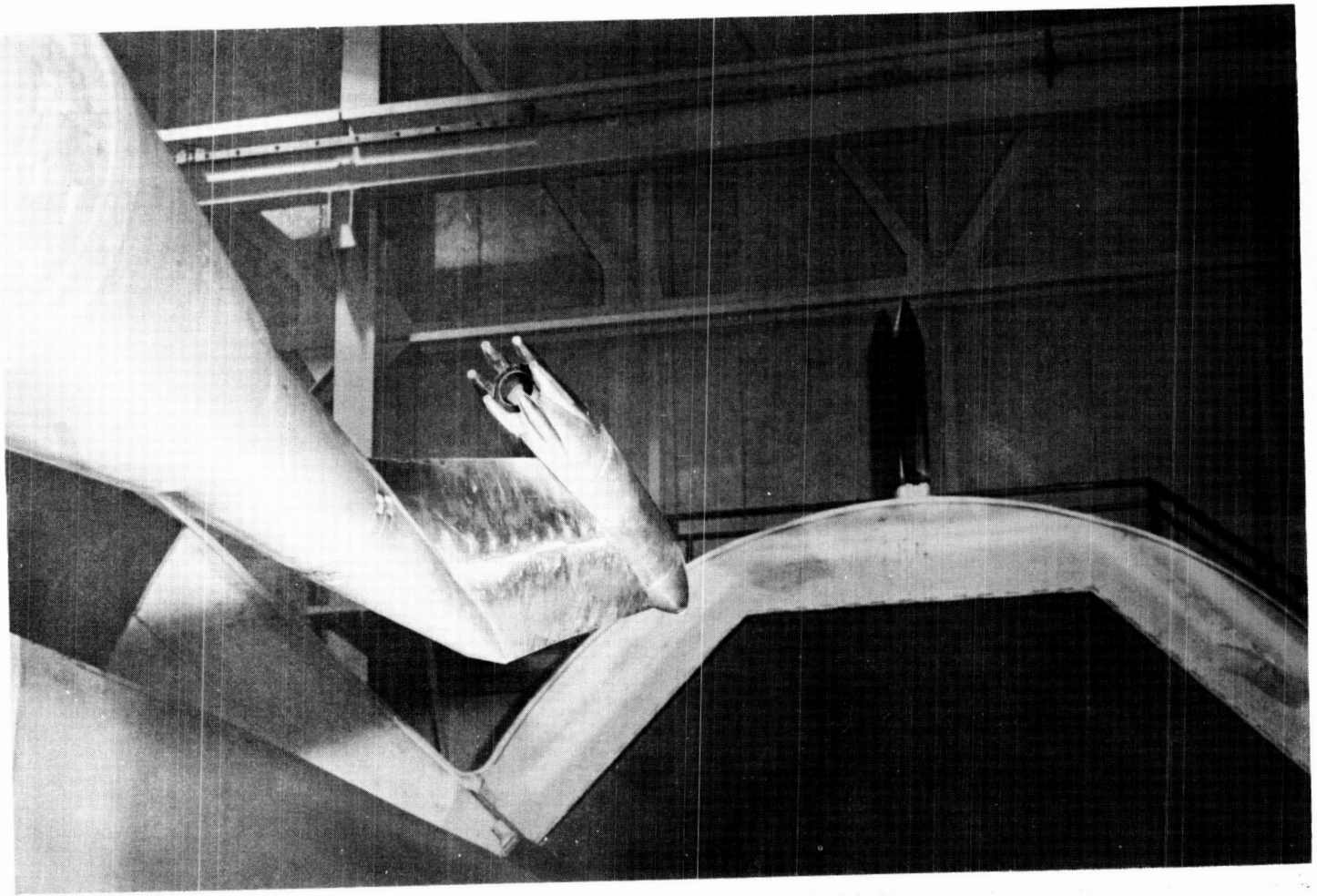

(b) Rear view. L-58-216

Figure 6.- Concluded.

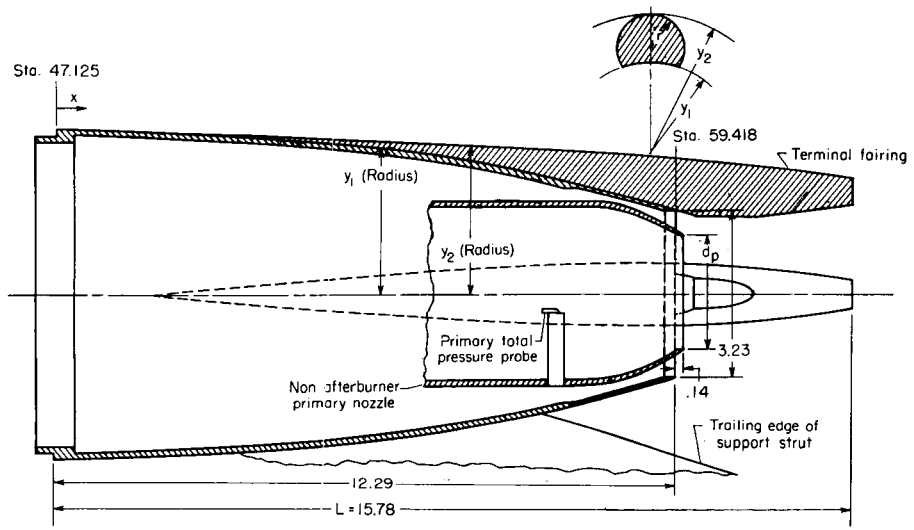

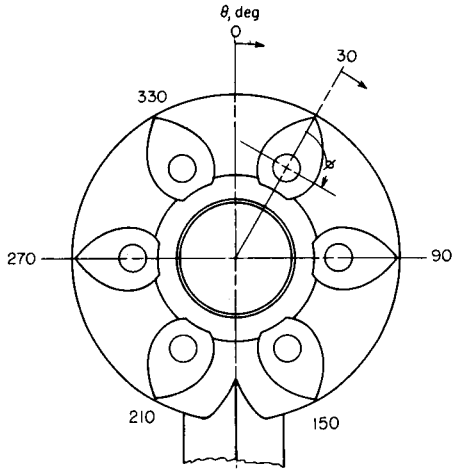

COORDINATES FOR TERMINAL FAIRINGS AND AFTERBODY				
Sta.	x	y_1	y_2	r
47.125	0.000	3.250		
48.000	.875	3.228		
49.000	1.875	3.189	3.189	0.600
50.000	2.875	3.143	3.149	.600
51.000	3.875	3.093	3.108	.600
52.000	4.875	3.018	3.066	.600
53.000	5.875	2.934	3.023	.600
54.000	6.875	2.825	2.978	.600
55.000	7.875	2.677	2.930	.600
56.000	8.875	2.495	2.881	.600
57.000	9.875	2.293	2.829	.600
58.000	10.875	2.038	2.775	.600
59.000	11.875	1.765	2.718	.600
59.418	12.293	1.632	2.692	.600
60.000	12.875	1.491	2.655	.600
61.000	13.875	1.491	2.570	.515
62.000	14.875		2.455	.400
62.907	15.782		2.326	.271

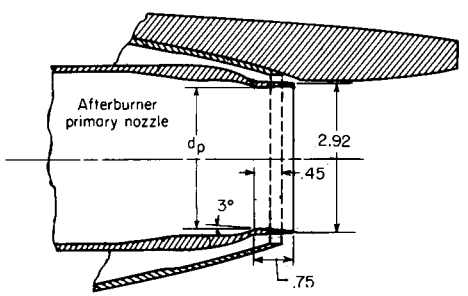

STATIC ORIFICE LOCATIONS ON TERMINAL FAIRINGS AND AFTERBODY					
	x	x/L		x	x/L
Fairings at $\theta = 30°$ and 210° Row at $\phi = 0°$	0.78	0.050	Fairings at $\theta = 150°$ and 330° Row at $\phi = 90°$	6.78	0.430
	3.78	.240		8.78	.556
	6.78	.430		10.78	.683
	8.78	.556		12.28	.778
	10.78	.683		13.58	.861
	12.28	.778		14.78	.937
	13.58	.861		15.68	.994
	14.78	.937			
	15.68	.994	Row on afterbody at $\theta = 0°$	0.79	0.050
	15.78	1.000		3.79	.240
				6.29	.399
				7.79	.494
Fairings at $\theta = 90°$ and 270° Row at $\phi = 180°$	13.18	0.835		9.29	.589
	13.88	.880		10.29	.652
	14.58	.924		11.29	.716
	15.28	.968		12.29	.779
	15.68	.994			

Figure 7.- Sketch of terminal-fairing-afterbody configuration. All dimensions are in inches.

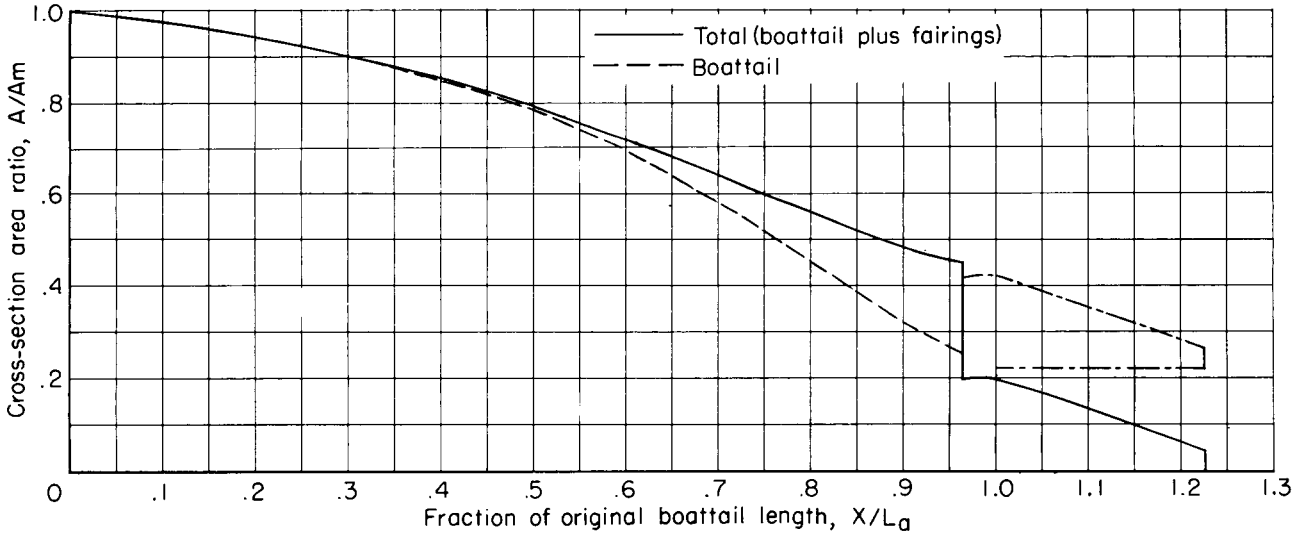

(a) Area progression.

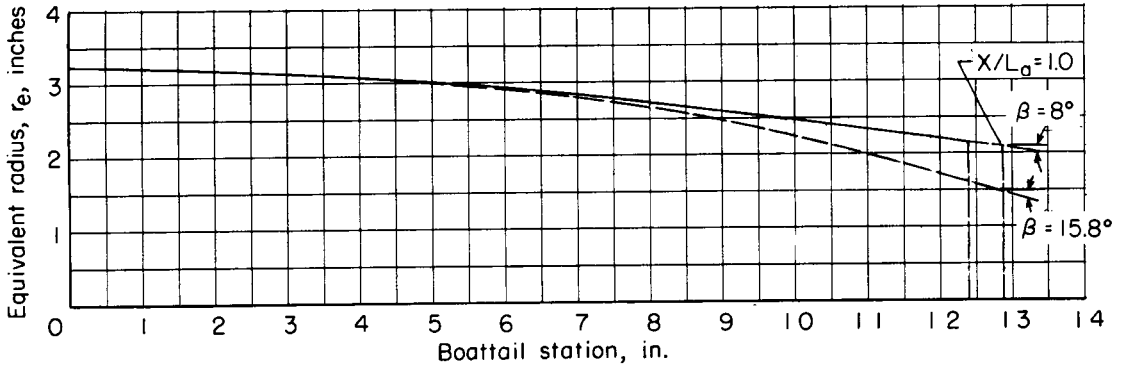

(b) Equivalent radius.

Figure 8.- Terminal-fairing-model area progression.

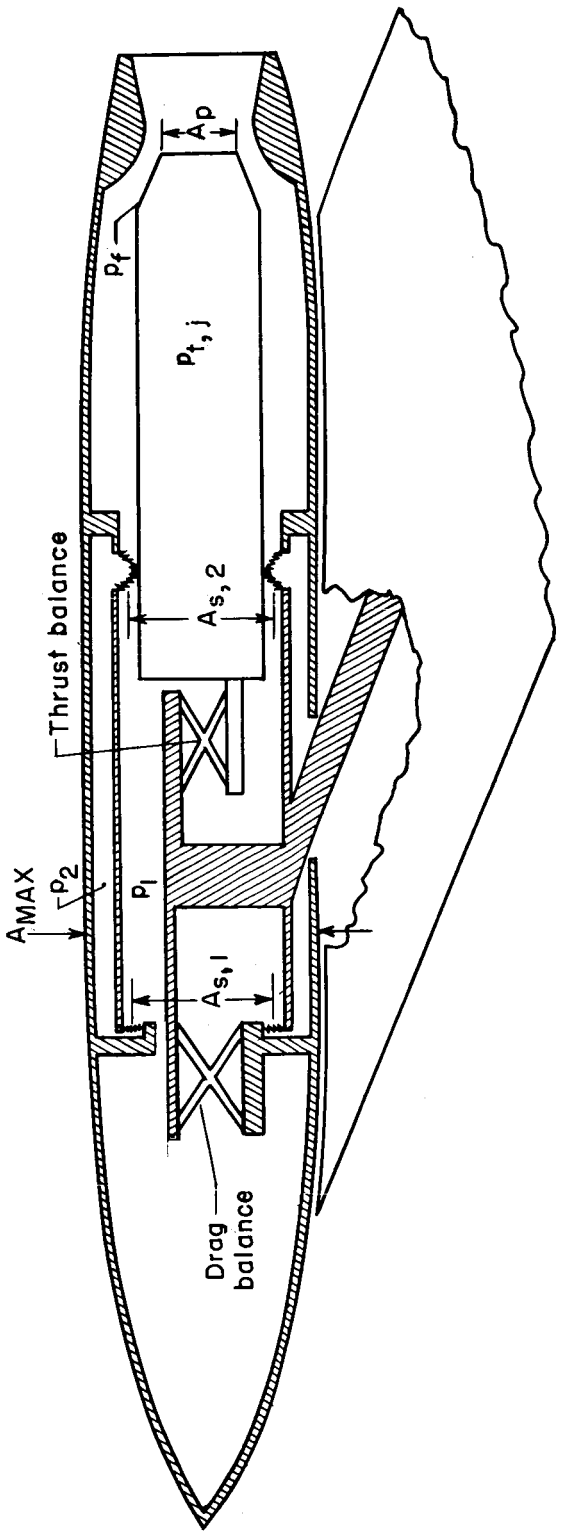

Figure 9.- Schematic diagram of thrust and drag systems.

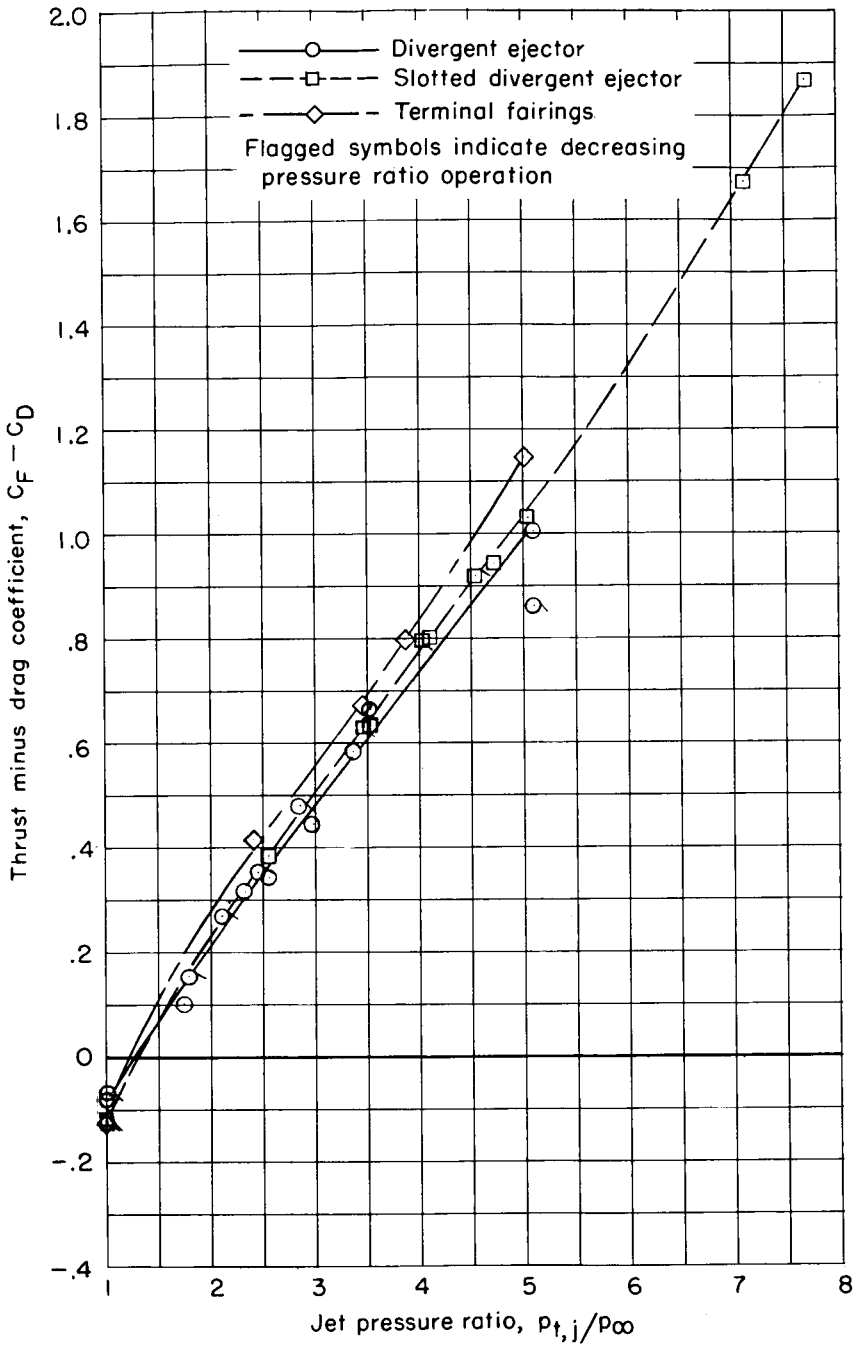

(a) $M_\infty = 0.80$.

Figure 10.- Variation of thrust minus drag coefficient with jet pressure ratio for the fixed afterbody models. Nonafterburner nozzle configuration.

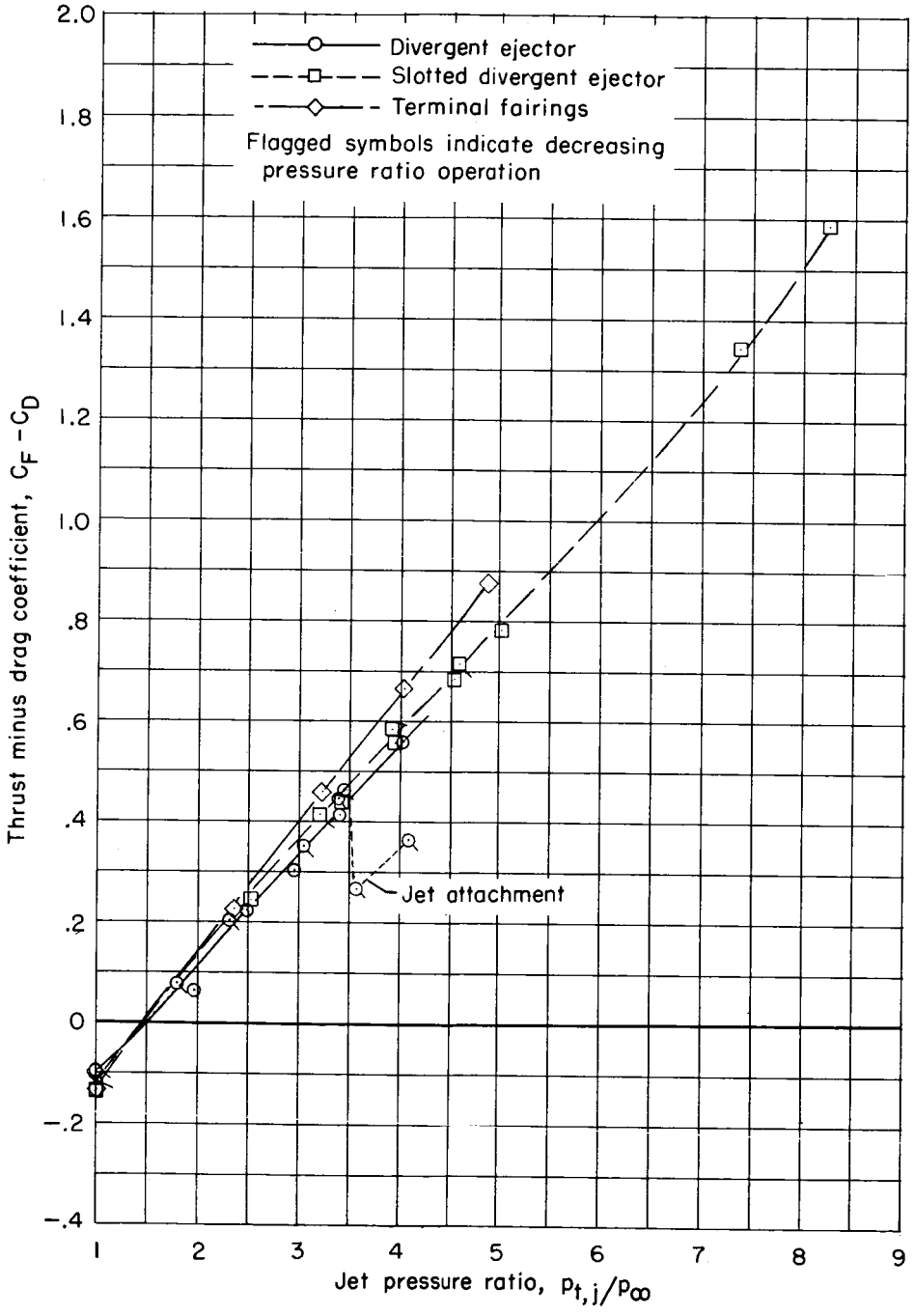

(b) $M_\infty = 0.90$.

Figure 10.- Continued.

[redacted]

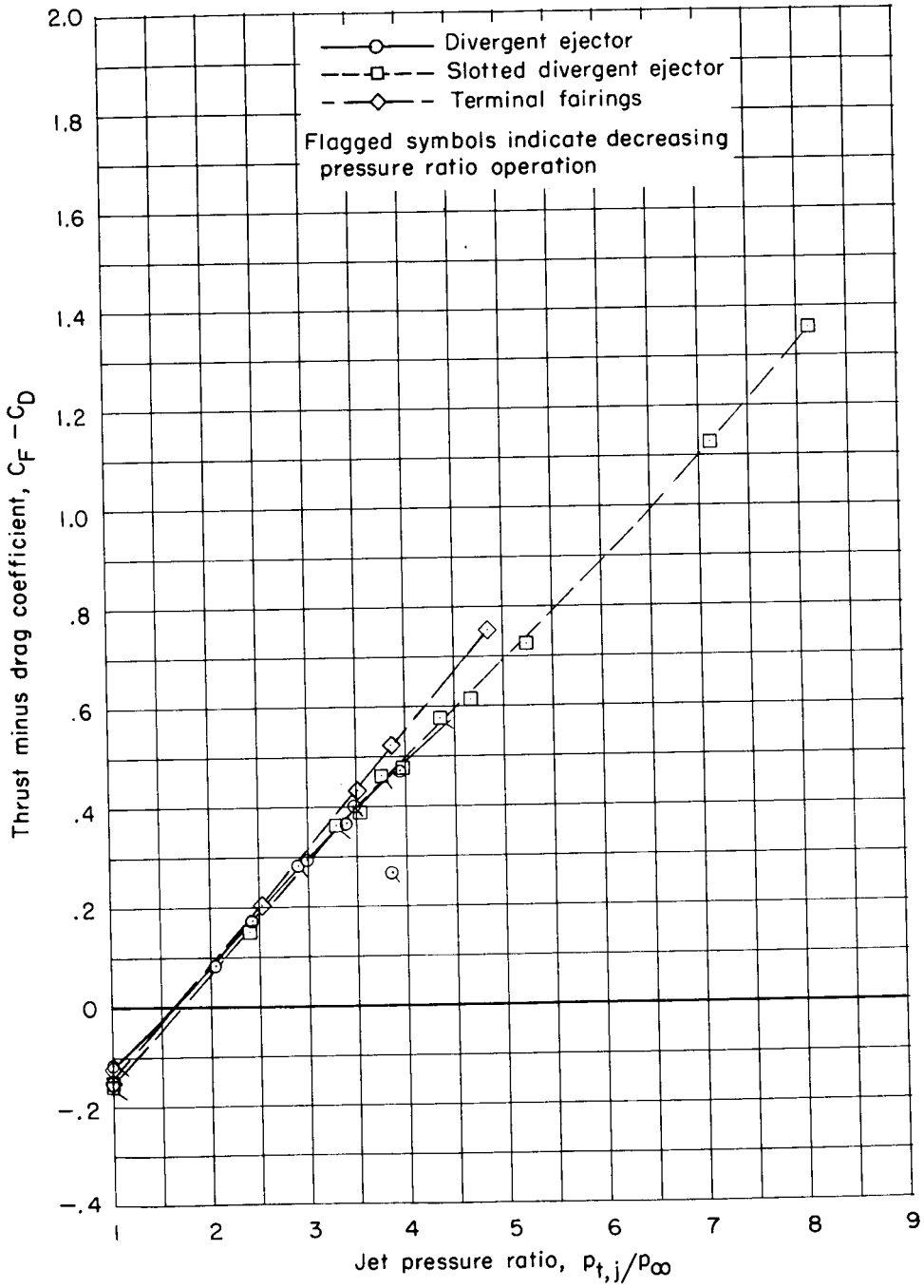

(c) $M_\infty = 0.95$.

Figure 10.- Continued.

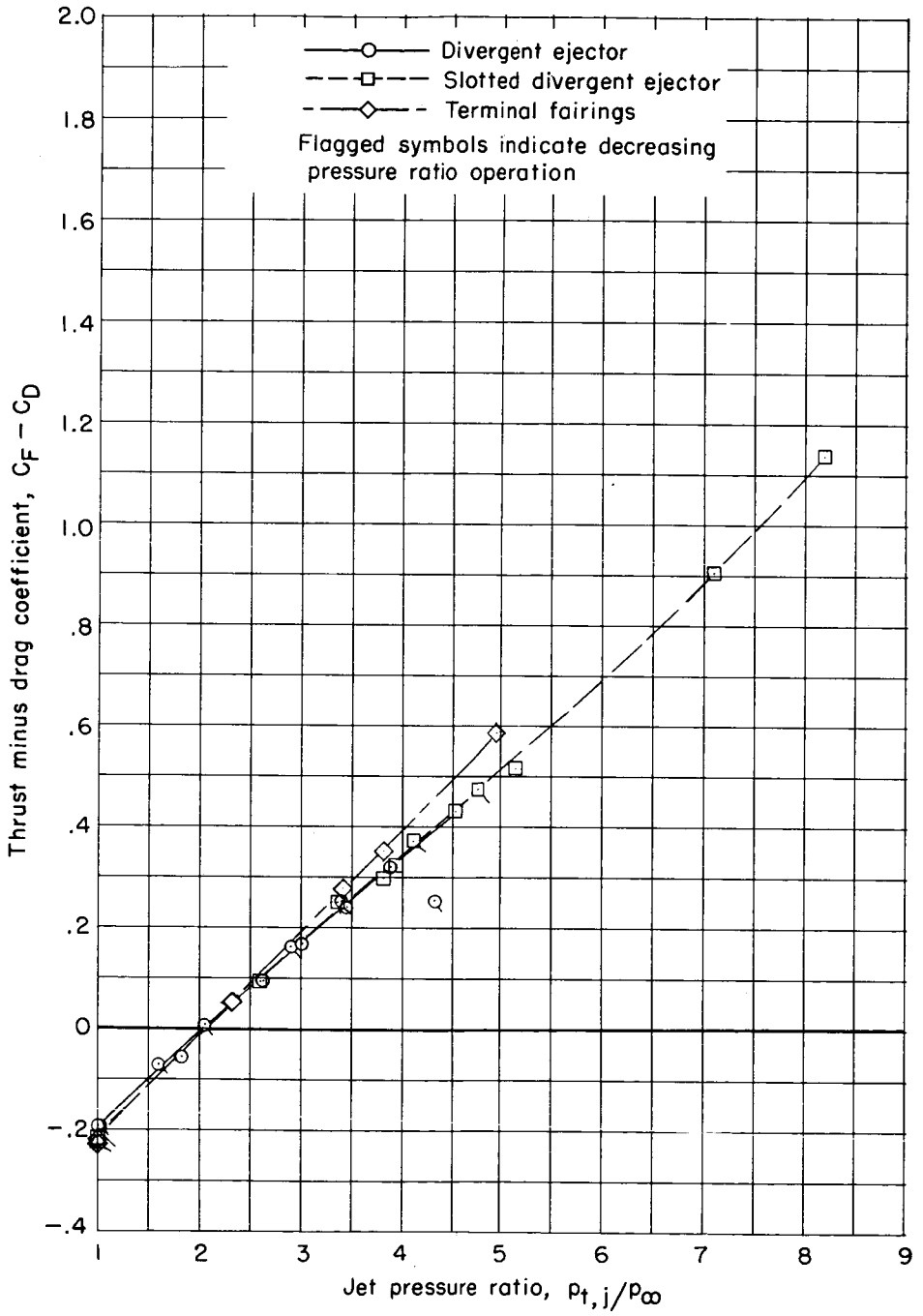

(d) $M_\infty = 1.00$.

Figure 10.- Continued.

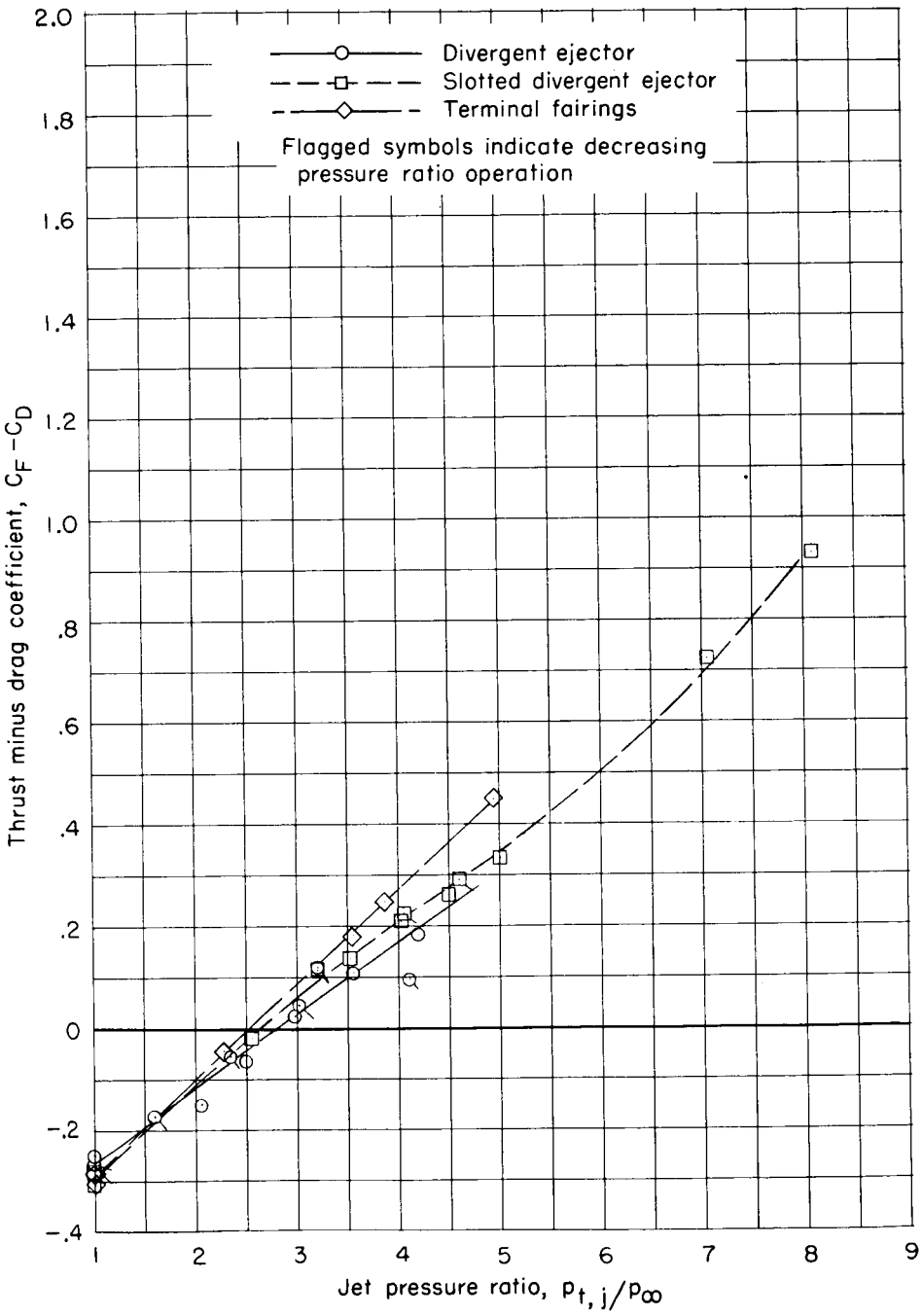

(e) $M_\infty \approx 1.05$ (divergent ejector $M_\infty = 1.00$).

Figure 10.- Concluded.

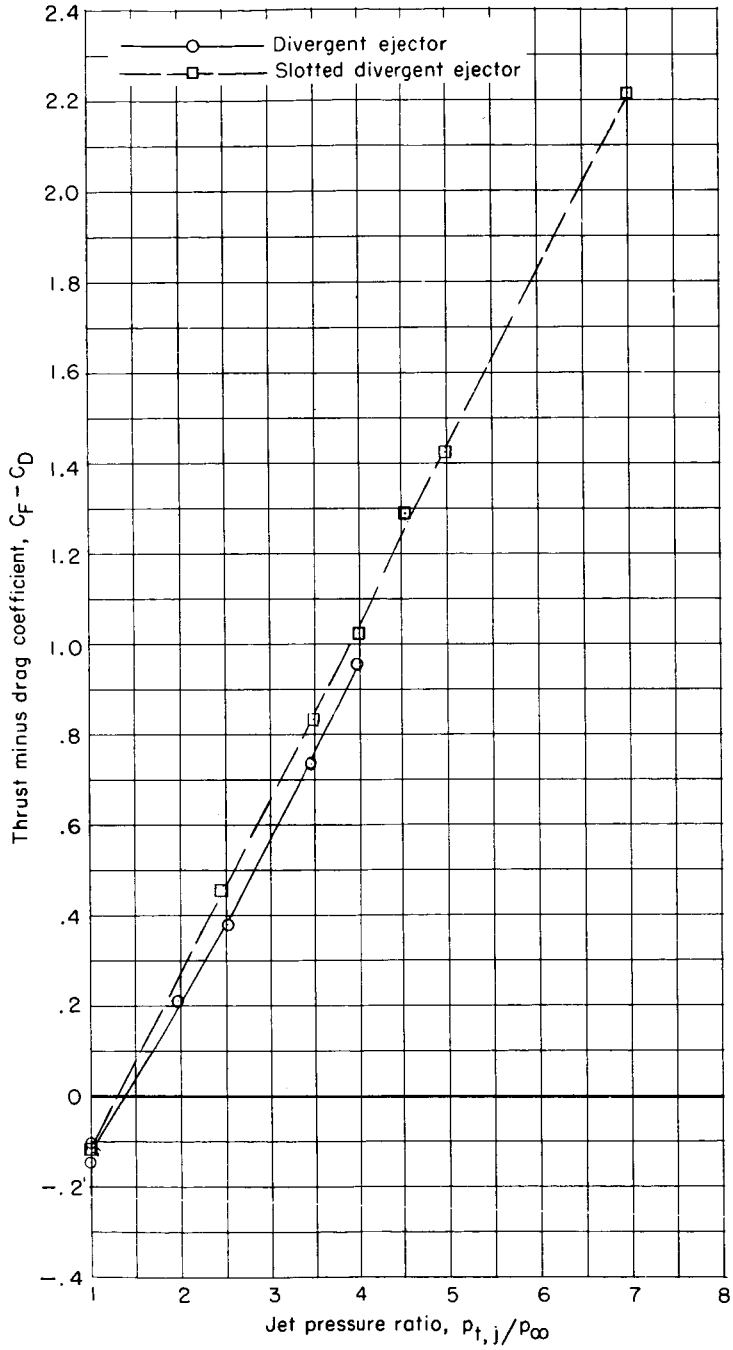

(a) $M_\infty = 0.90$.

Figure 11.- Variation of thrust minus drag coefficient with jet pressure ratio for the three fixed afterbody models. Afterburner nozzle configurations.

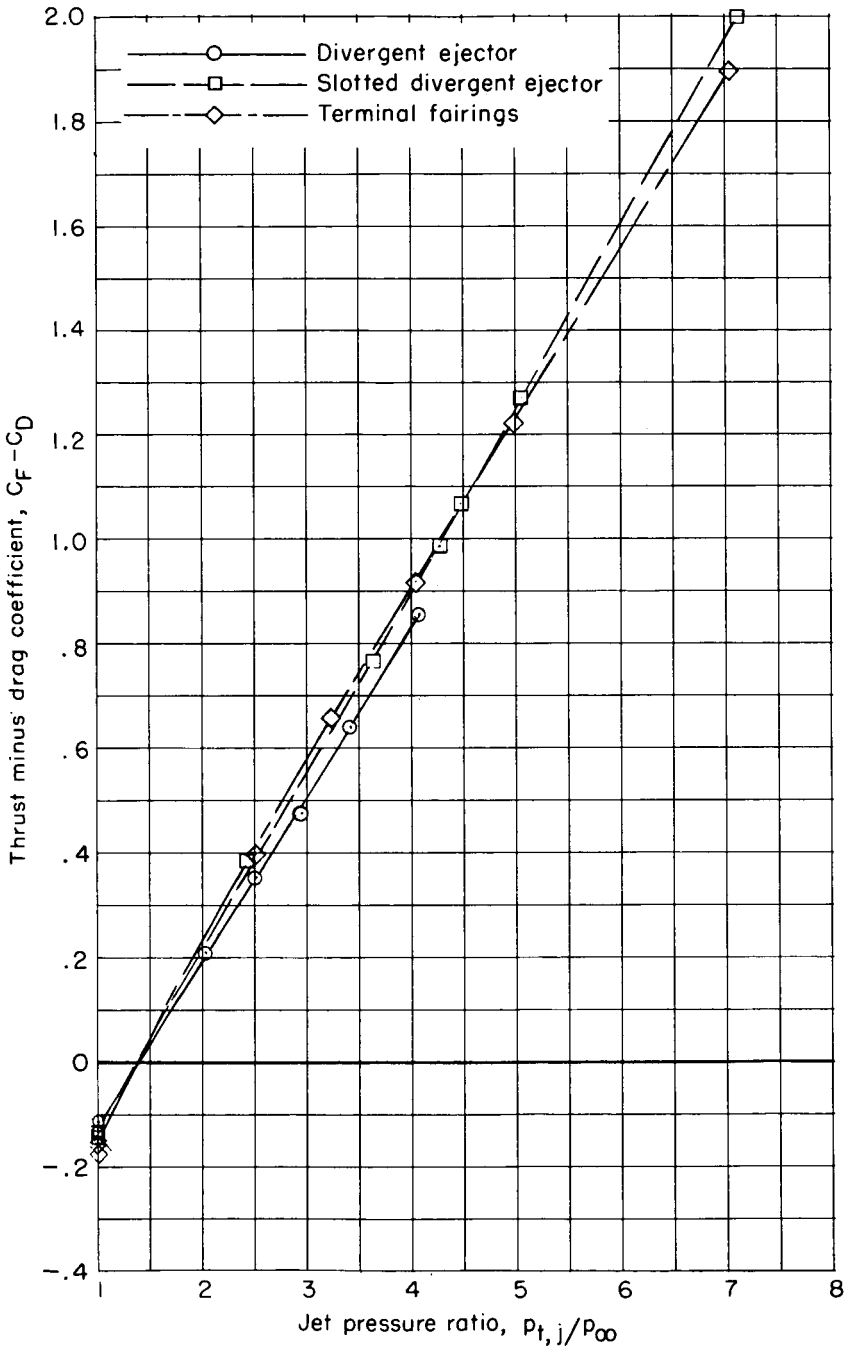

(b) $M_\infty = 0.95$.

Figure 11.- Continued.

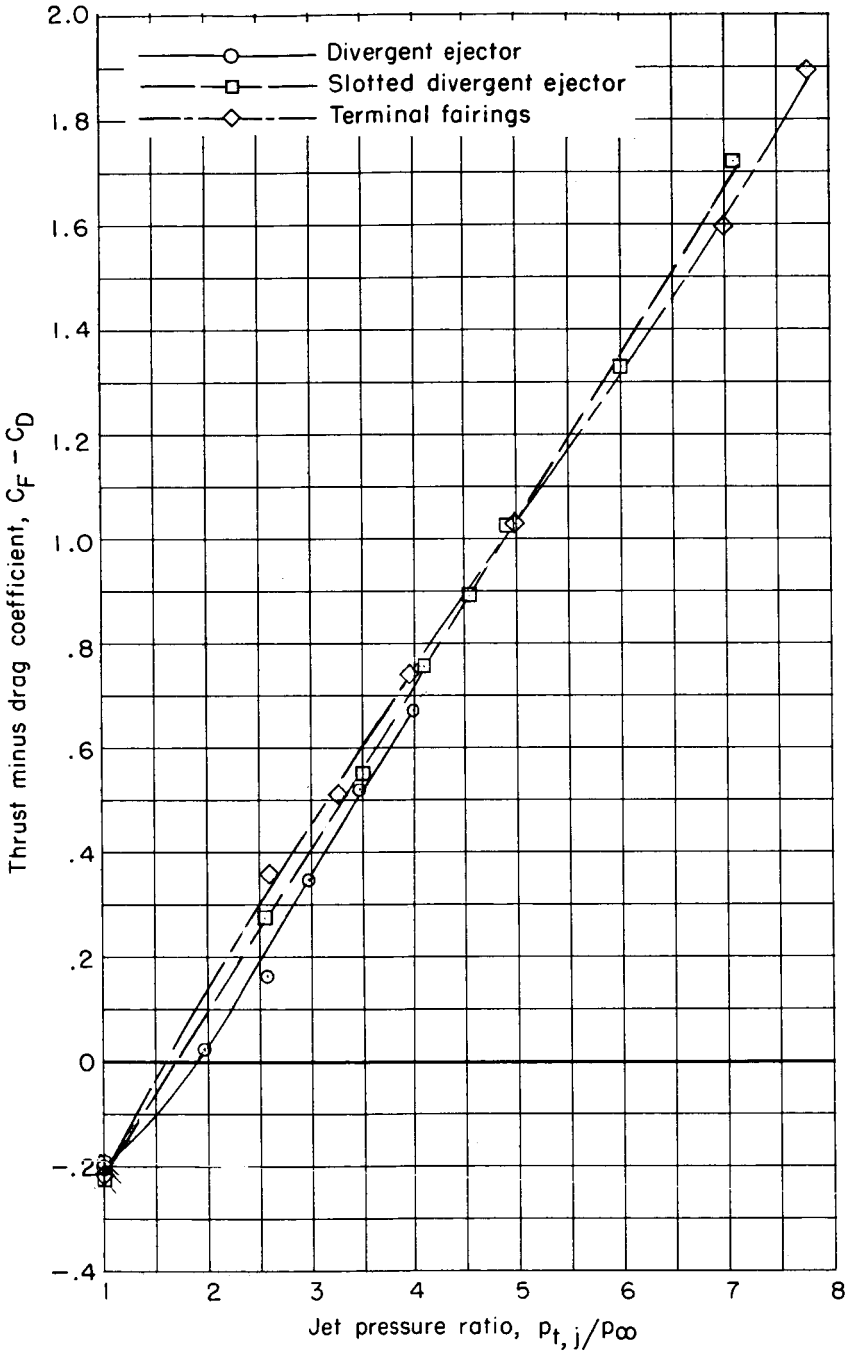

(c) $M_\infty = 1.00$.

Figure 11.- Continued.

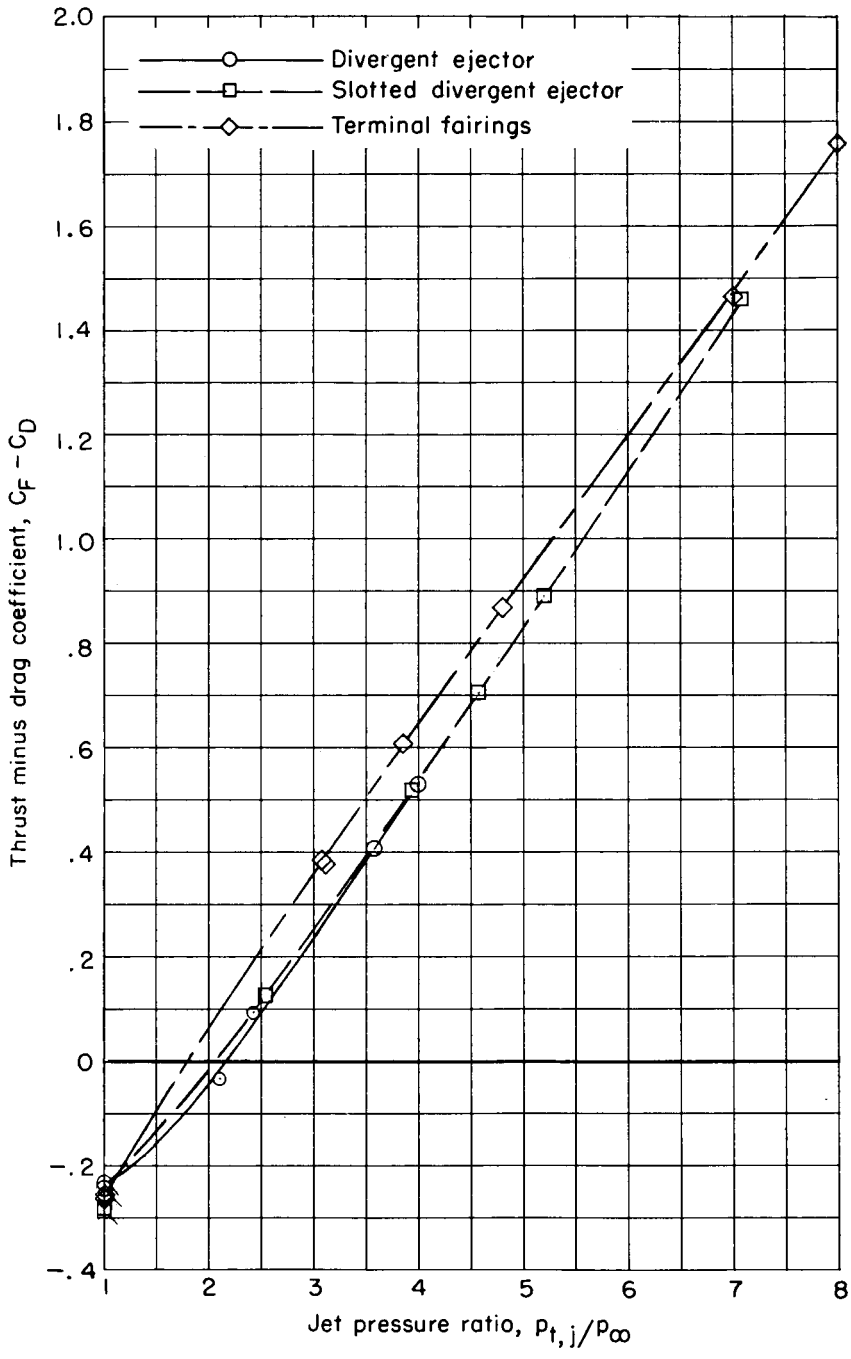

(d) $M_\infty \approx 1.05$ (divergent ejector $M_\infty = 1.06$).

Figure 11.- Concluded.

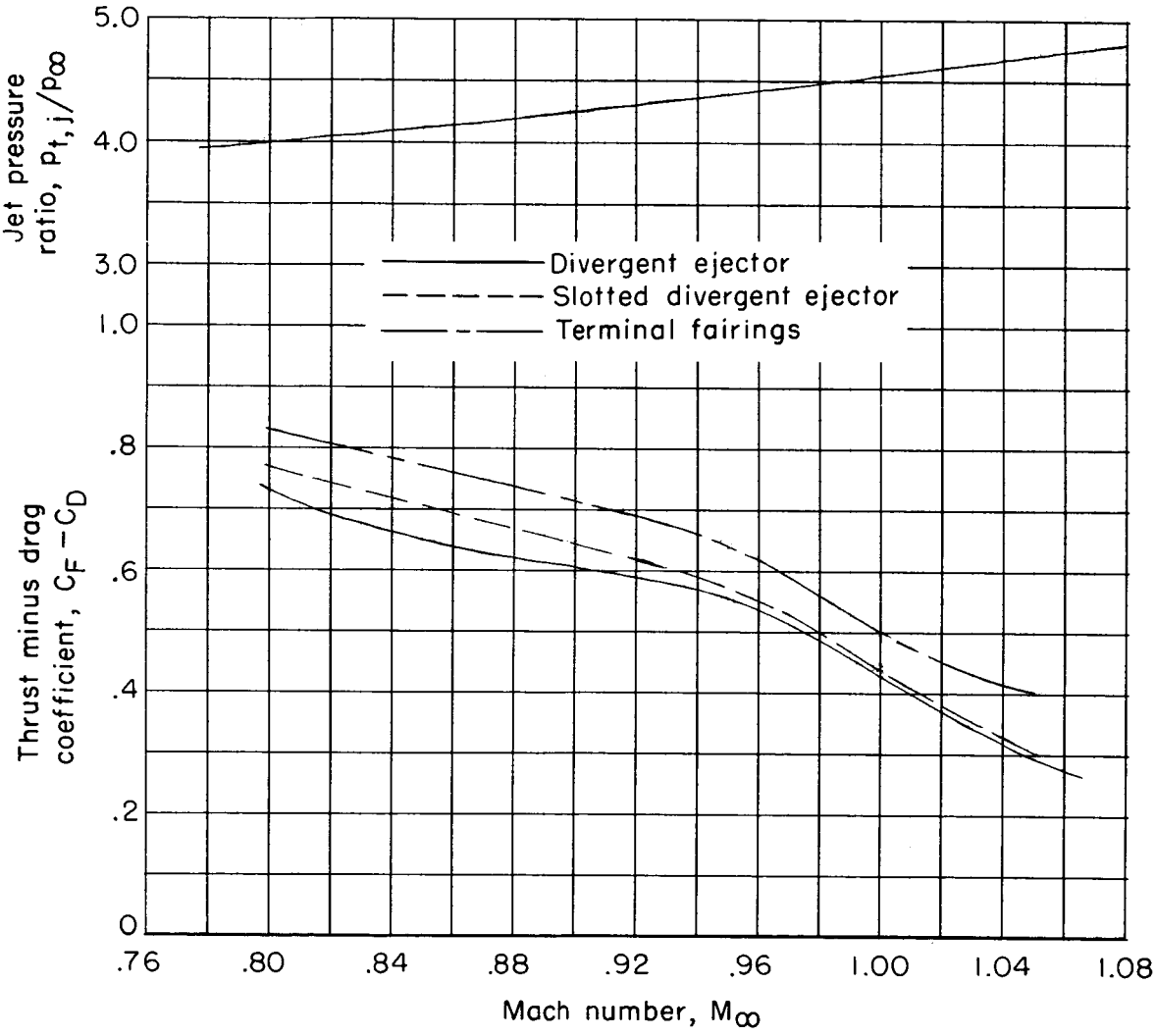

Figure 12.- Variation of thrust minus drag coefficient with Mach number for the fixed afterbody models at a scheduled jet pressure ratio. Nonafterburner nozzle configurations.

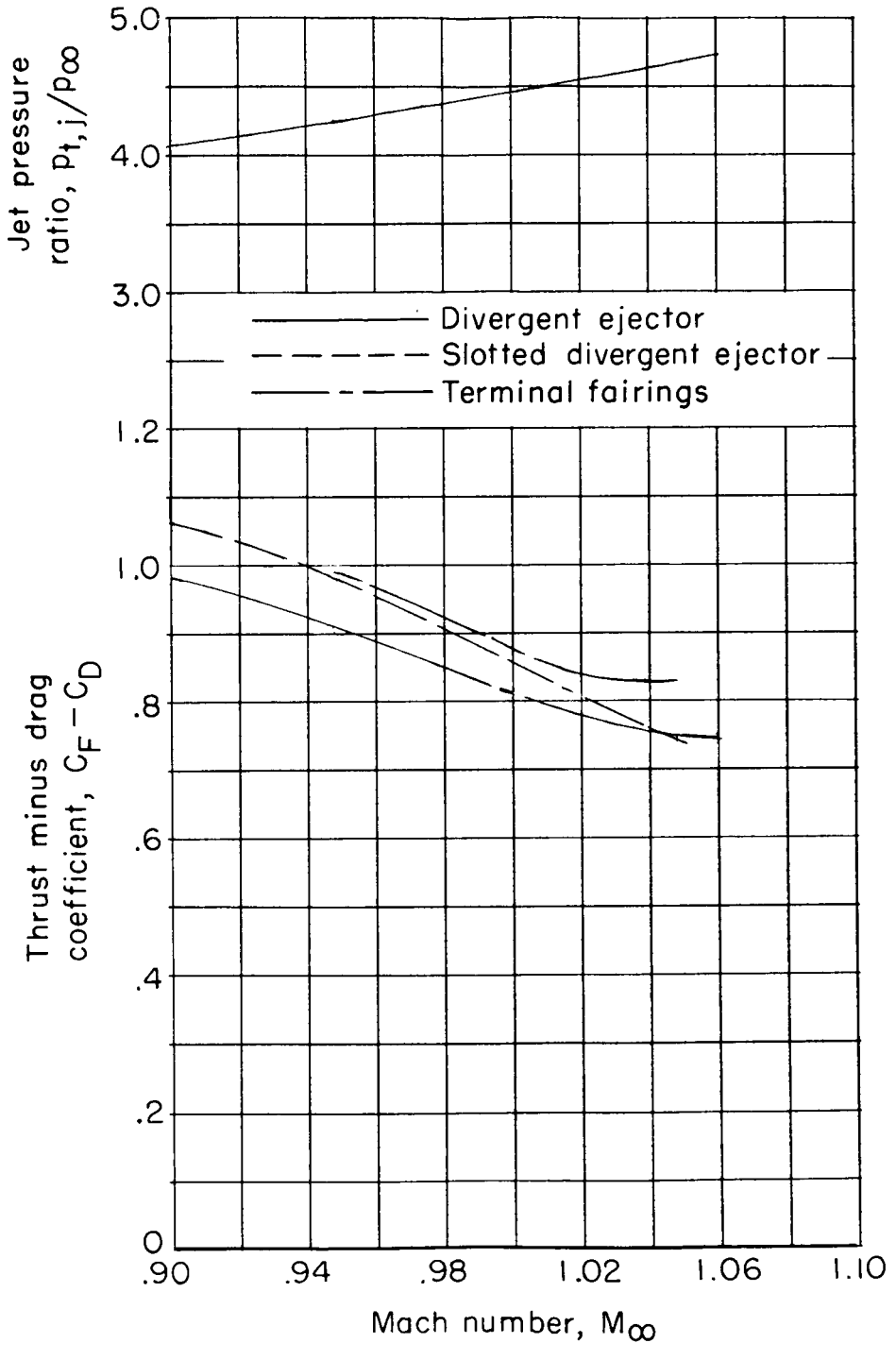

Figure 13.- Variation of thrust minus drag coefficient with Mach number for the fixed afterbody models at a scheduled jet pressure ratio. Afterburner nozzle configurations.

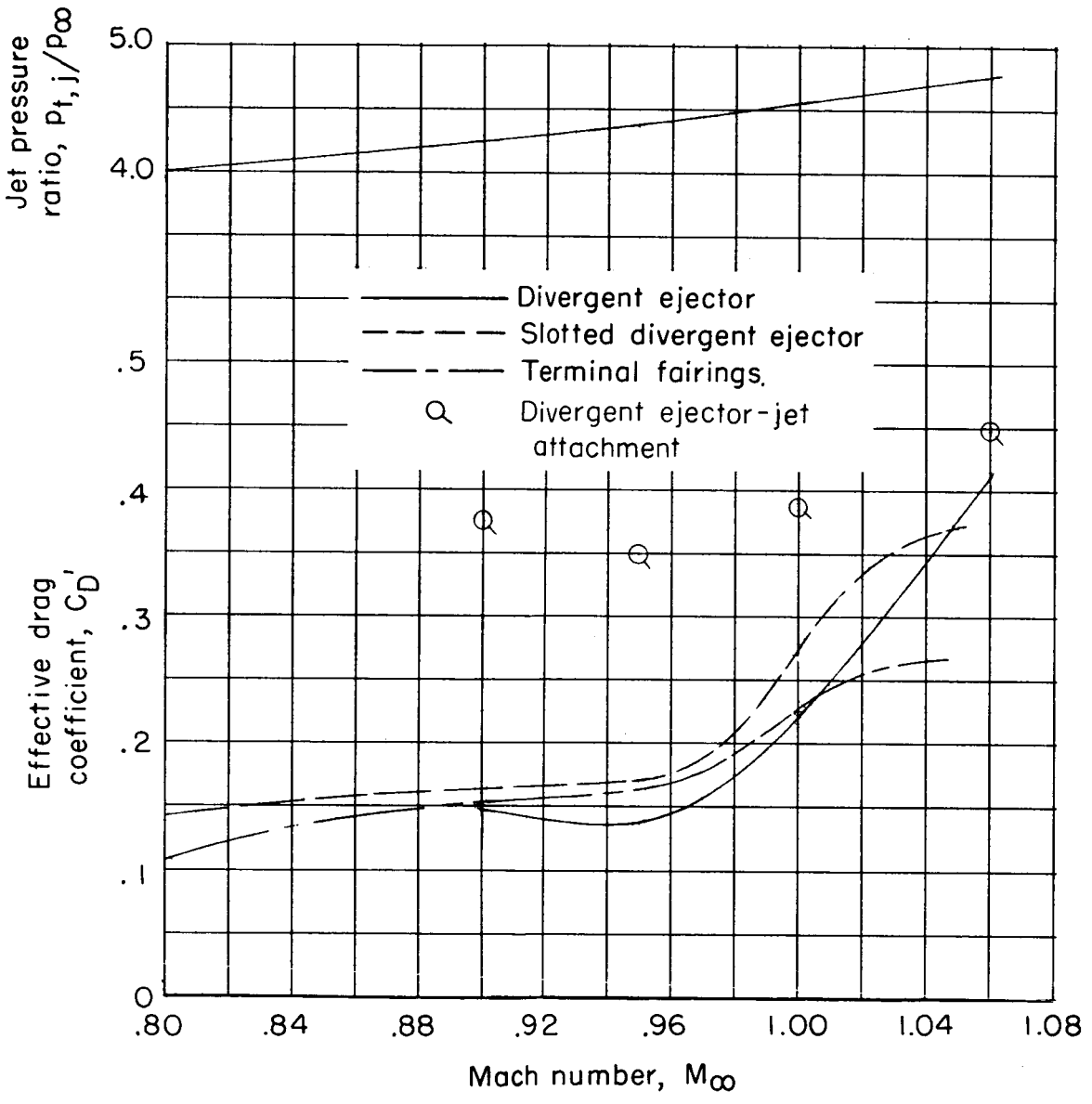

Figure 14.- Variation of effective drag coefficient with Mach number for the three fixed afterbody models at a scheduled jet pressure ratio. Nonafterburner nozzle configurations.

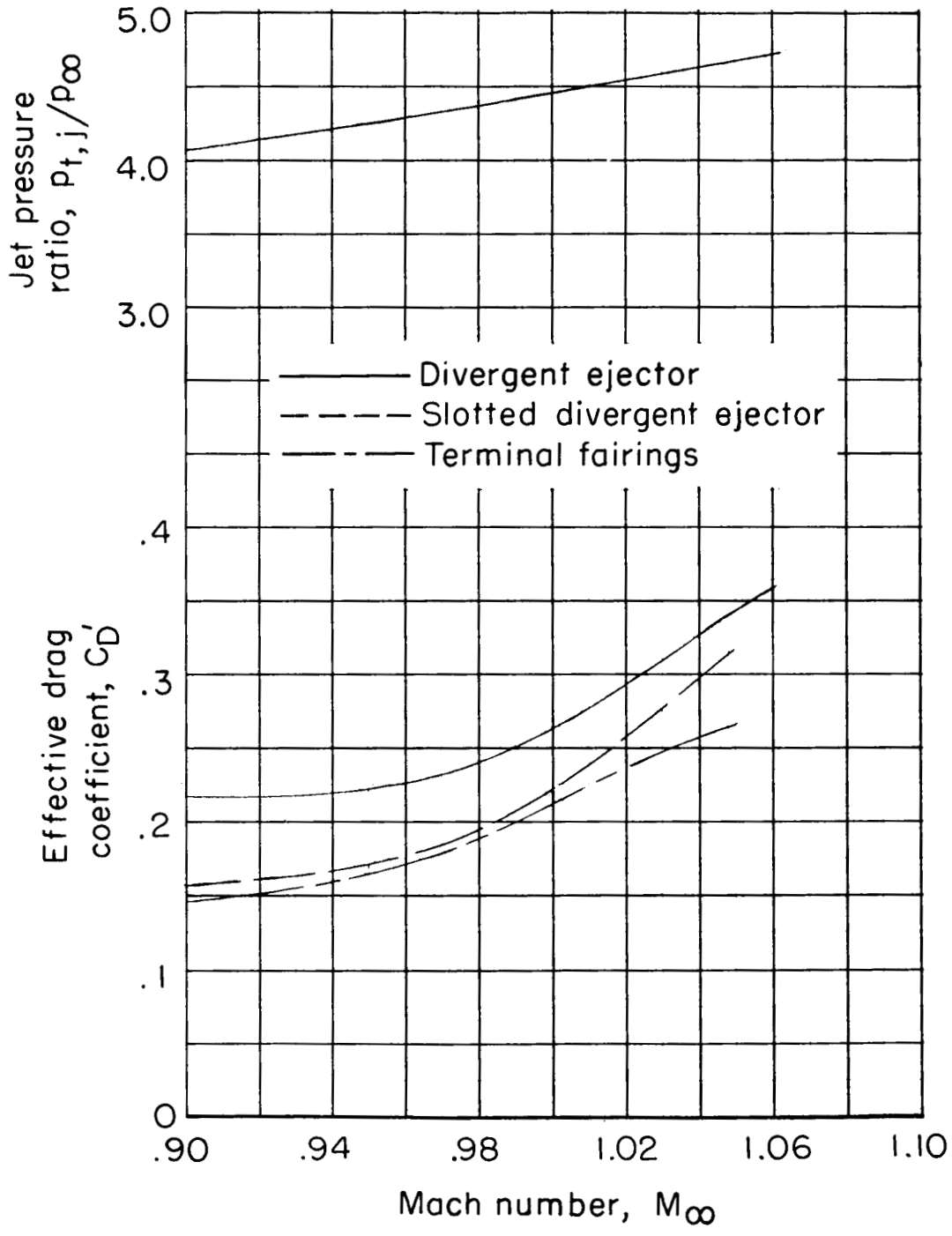

Figure 15.- Variation of effective drag coefficient with Mach number for the three fixed afterbody models at a scheduled jet pressure ratio. Afterburner nozzle configurations.

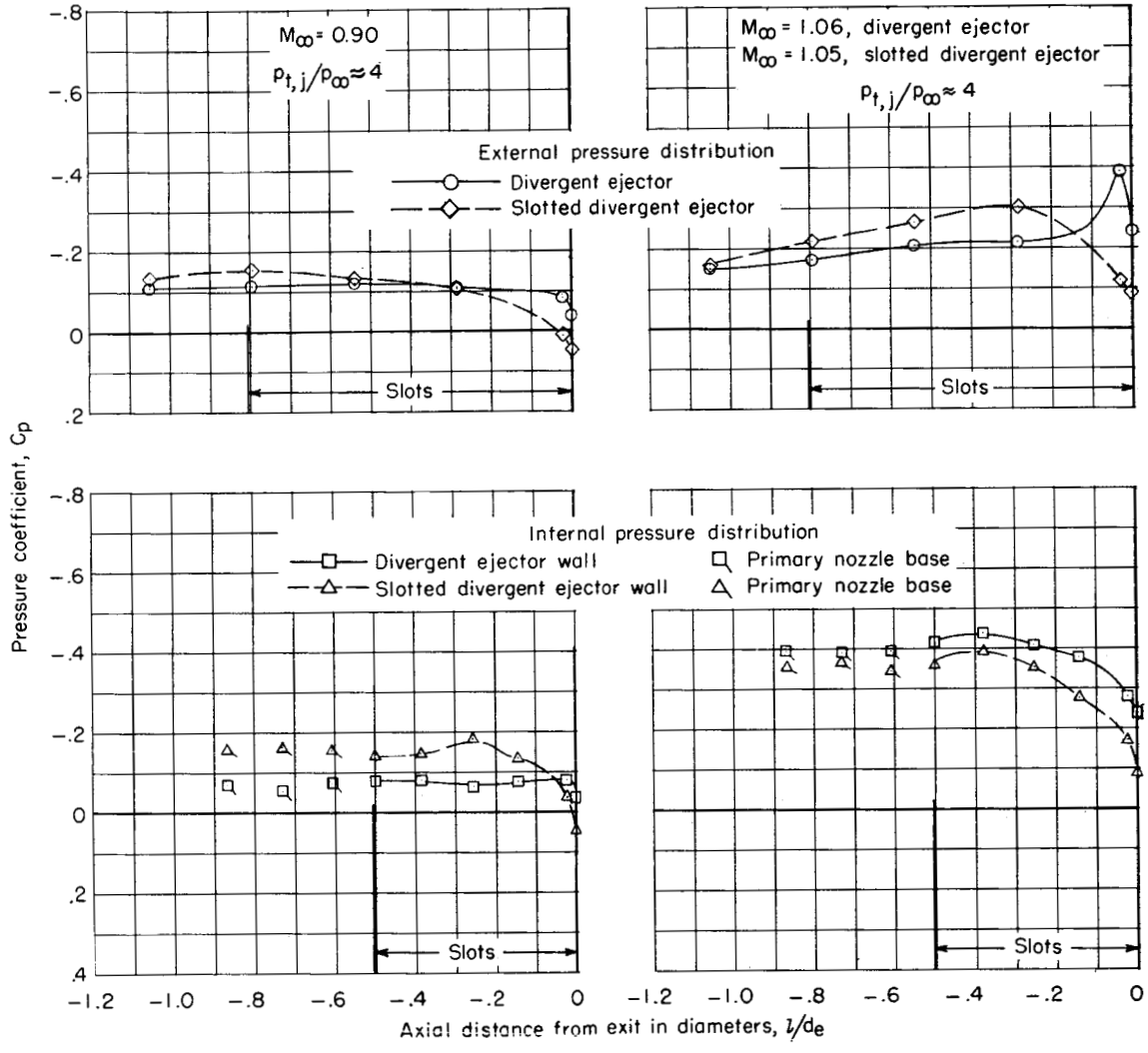

(a) Nonafterburner nozzles.

Figure 16.- Typical pressure distributions obtained over rear portions of divergent ejector and slotted divergent ejector configurations.

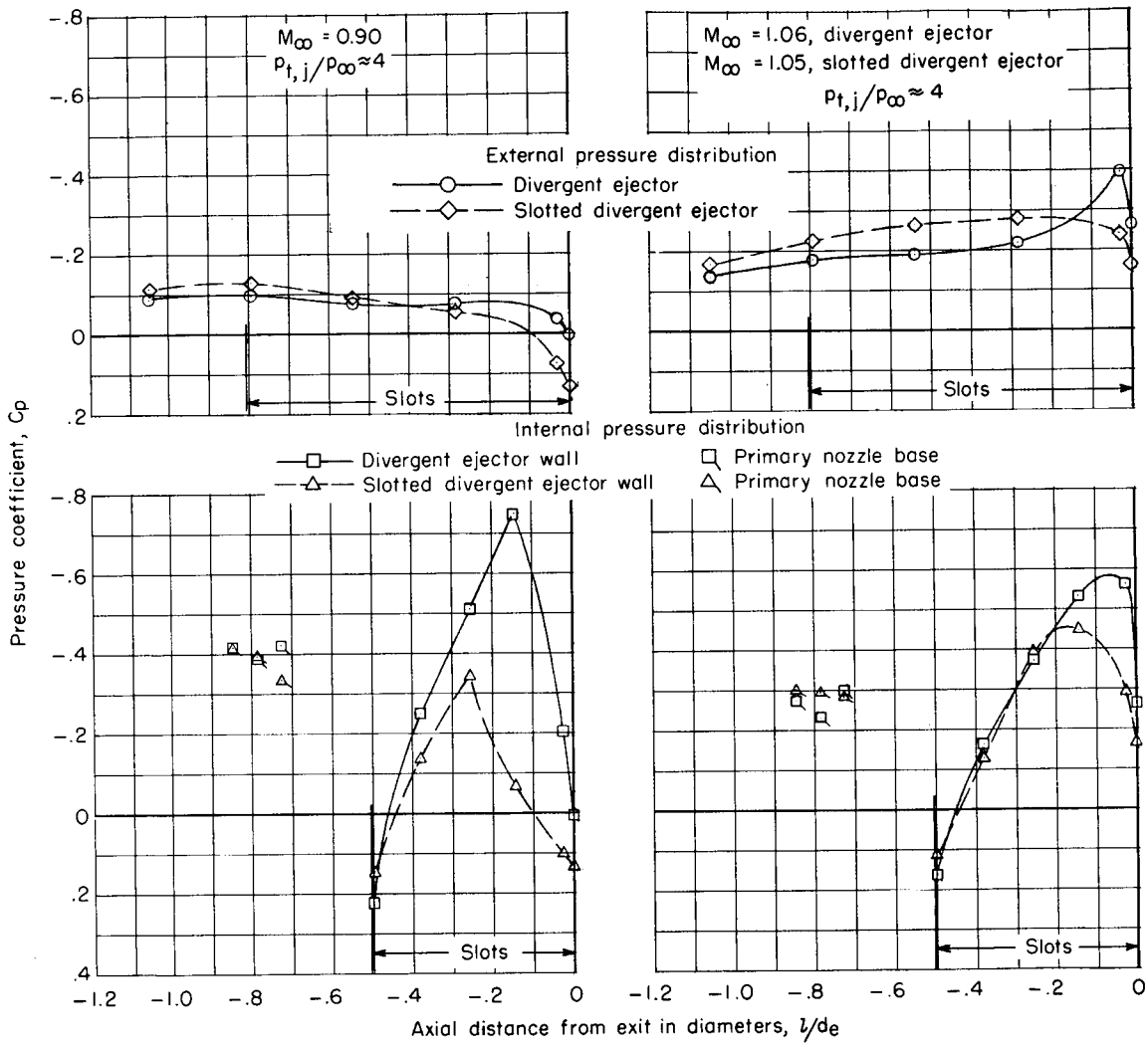

(b) Afterburner nozzles.

Figure 16.- Concluded.

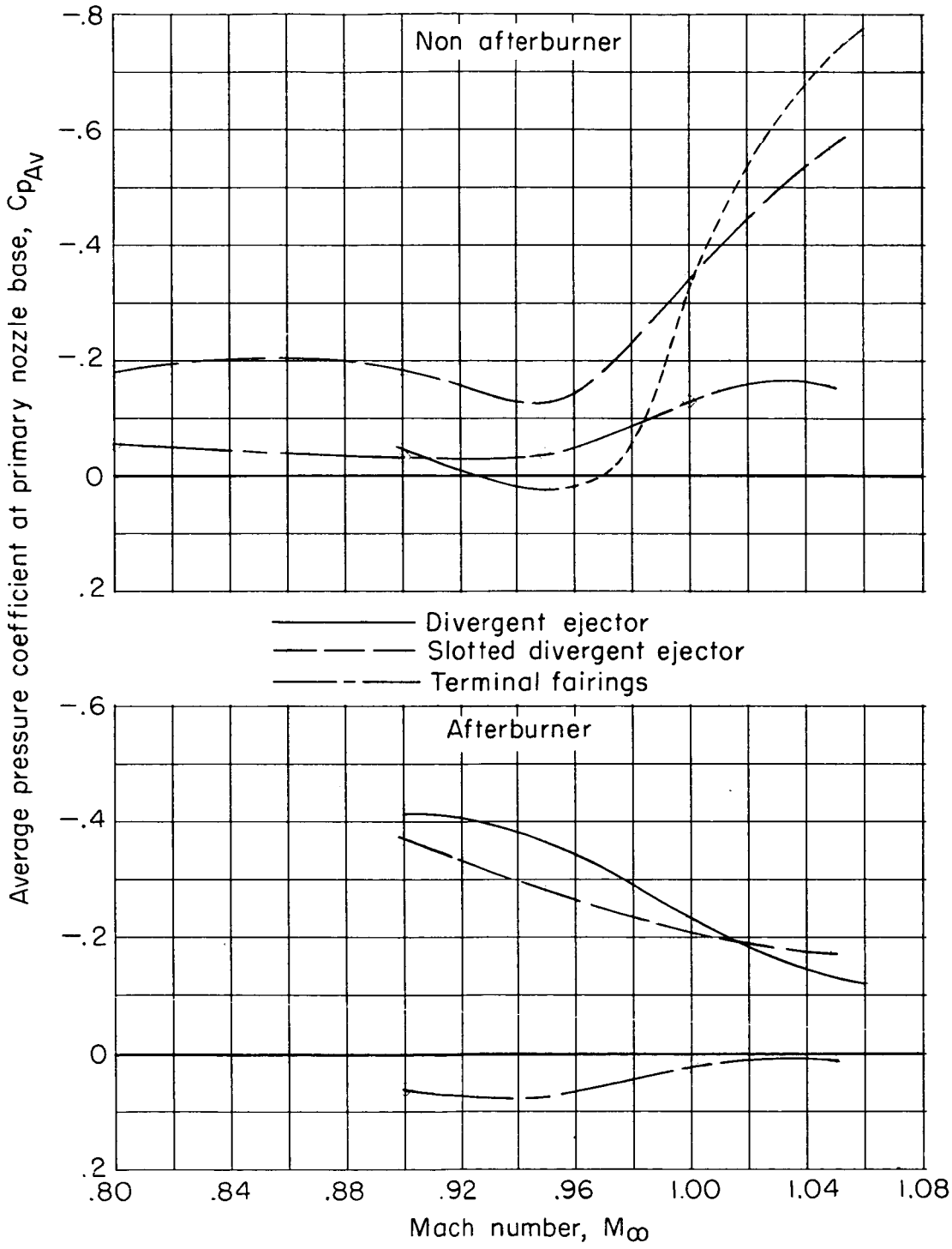

Figure 17.- Variation in average pressure coefficient at the primary nozzle base with Mach number for scheduled jet pressure ratios.